9

Wood Physics/Mechanical Properties

Sara Florisson* and Erik Kristofer Gamstedt

An overview of lab-based micro computed tomography aided finite element modelling of wood and its current bottlenecks

https://doi.org/10.1515/hf-2023-0061 Received June 12, 2023; accepted October 4, 2023; published online November 9, 2023

Abstract: Microscopic lab-based X-ray computed tomography (XµCT) aided finite element (FE) modelling is a popular method with increasing nature within material science to predict local material properties of heterogeneous materials, e.g. elastic, hygroexpansion and diffusion. This method is relatively new to wood and lacks a clear methodology. Research intended to optimise the XµCT aided FE process often focuses on specific aspects within this process such as the XµCT scanning, segmentation or meshing, but not the entirety of the process. The compatibility and data transfer between aspects have not been investigated to the same extent, which creates errors that propagate and negatively impact the end results. In the current study, a methodology for the XµCT aided FE process of wood is suggested and its bottlenecks are identified based on a thorough literature review. Although the complexity of wood as a material makes it difficult to automate the XµCT aided FE process, the proposed methodology can assist in a more considered design and execution of this process. The main challenges that were identified include an automatic procedure to reconstruct the fibre orientation and to perform segmentation and meshing. A combined deep-learning segmentation method with geometry-based meshing can be suggested.

Keywords: X-ray computed tomography; wood; process improvement methodology; segmentation; meshing; digital volume correlation

Erik Kristofer Gamstedt, Division of Applied Mechanics, Uppsala University, Ångströmlaboratoriet, Lägerhyddsvägen 1, 751 03, Uppsala, Sweden

1 Introduction

This section presents some main characteristics of computed tomography (CT), its use in wood material science, the relation to finite element (FE) analysis, and the topic of integrating these techniques. If wisely assembled, these tools provide a powerful system to gain more understanding in wood material mechanics, which can be used to solve engineering problems. With this work, we would like to give an overview and to identify and highlight some of the challenges in construing such an integrated methodology in a broader context, since available research in the area is predominantly focused on separate segments and not on the potential coherent framework.

1.1 Introduction to CT

Ionising radiation CT, such as X-ray CT and γ -ray CT, can be used to determine the heterogeneous structure of materials in a non-destructive and non-invasive manner providing three-dimensional (3D) and four-dimensional (4D, 3D + time) information (Bucur 2003). The technique gives detailed tomograms reconstructed from two-dimensional (2D) radiographs, with greyscale information at each voxel (volume element). A radiograph is an image formed by digitally collected transmitted X-rays through an object, whereas greyscale indicates the range of voxel values within a tomographic data set (Withers et al. 2021). Radiographs of an object at a given angle are called projections, which combined allow for a 3D reconstruction of the object.

The most critical resolutions in CT scanning are *spatial*, *contrast* and *temporal* resolution. Spatial resolution refers to the size of the smallest possible feature that can be detected inside a tomogram. As a rule of thumb, three times the pixel size can be assumed (Lindgren 1992). The contrast resolution quantifies the ability to accurately measure slight differences in density between neighbouring regions within a tomogram, whereas temporal resolution is defined as the amount of time needed to capture two consecutive

S. Florisson and E. K. Gamstedt: Lab-based micro computed tomography aided FE modelling of wood.

^{*}Corresponding author: Sara Florisson, Division of Applied Mechanics, Uppsala University, Ångströmlaboratoriet, Lägerhyddsvägen 1, 751 03, Uppsala, Sweden, E-mail: sara.florisson@angstrom.uu.se. https://orcid.org/0000-0001-7322-7052

tomograms (Lindgren 1992; Withers et al. 2021). For high (spatial) resolution microscopic (micro) CT, the voxel size is generally >0.1 µm (micron) and for low resolution macroscopic (macro) CT, the voxel size is generally >100 um. A smaller voxel size inevitably necessitates a smaller specimen, hence the difference in specimen size between industrial and lab-based scanners.

X-ray µCT is becoming increasingly popular in material science (e.g. Auenhammer et al. 2022; Buljac et al. 2018; Salvo et al. 2003; Stock 2013; Zauner 2014), since it allows for the structural characterisation of heterogeneous materials at the micro material level. This ability makes it highly suitable for wood. At the micro material level, a direct correlation can be seen between the length, diameter and shape of the wood tracheids and its density and hygromechanical behaviour (Persson 2000). The most commonly used techniques for X-ray μCT are laboratory-based X-ray tube μCT (XμCT) and synchrotron radiation-based X-ray µCT (SRµCT). As the names suggest, the main difference between XµCT and SRµCT is the radiation source. XµCT uses an X-ray tube, whereas SRµCT uses a cyclic particle accelerator. Their beams differ in terms of X-ray flux, source size and X-ray energy spectrum. The tube sources used in XµCT emit a wide range of X-ray energy often in a cone shaped beam referred to as polychromatic. The scan times range between minutes to hours depending on the required resolutions. SRµCT can generate more flux than tube sources using a monochromatic beam (one X-ray energy). This creates a sensitivity to small differences in X-ray adsorption and limits certain artefacts (Withers et al. 2021). The scan time ranges from subseconds to minutes. Although XµCT is becoming rapidly faster (Zwanenburg et al. 2022), SRµCT is more suited when high temporal resolution is needed.

1.2 Brief summary of CT on wood

The investigation of wood with X-ray CT started in the mideighties (e.g. Hattori and Kanagawa 1985; Kanagawa and Hattori 1985; Lindgren 1988). Since then, a number of doctoral theses have been written on the analysis of wood using SRµCT (Forsberg 2008; Zauner 2014), XµCT (Modzel 2009) and macro CT (Couceiro 2019; Danvind 2005; Lindgren 1992; Rosenkilde 2002; Wiberg 1998). SRuCT has been used to predict the elastic micromechanical behaviour (Forsberg et al. 2008, 2010; Zauner 2014), hygroexpansion behaviour and properties (Derome et al. 2011; Keunecke et al. 2012), moisture content changes during drying (Couceiro et al. 2022) and damage evolution (Baensch et al. 2015; Zauner et al. 2016) of wood, as well as the micromechanics of wood adhesive bonds (Ching et al. 2018; Modzel 2009; McKinley

et al. 2016; Paris et al. 2014, 2015). XµCT has mainly been used to study the capillary water uptake during imbibition (Martin et al. 2022; Perré et al. 2022), moisture change in plywood (Li et al. 2014), to determine the hygroexpansion properties of wood (Badel and Perré 2001; Patera et al. 2018b) and to analyse the properties of wood fibres in composites (Joffre et al. 2014, 2017). XµCT has also been used to analyse resin distribution in wood fibre boards (Kibleur et al. 2022a). the swelling of wood fibre boards (Kibleur et al. 2022b), and the water transport in medium-density fibre boards and oriented strand board (Li et al. 2013). X-ray macro CT has been used for the analysis of moisture content change during drying of timber (Couceiro et al. 2020; Hattori and Kanagawa 1985; Kanagawa and Hattori 1985; Lazarescu et al. 2010; Lindgren 1991b; Lindgren et al. 2016; Watanabe et al. 2012), the reconstruction of orthotropic material orientation (Huber et al. 2022), and knot detection (Fredriksson et al. 2019).

1.3 XµCT aided FE modelling

XμCT aided FE modelling uses XμCT data for fast and accurate prediction of critical parameters for modelling. Adopting suitable image-processing techniques, the method uses information from tomograms to create e.g., the geometry of the model, orthotropic material orientation, and boundary conditions, and to perform needed model calibrations and validations (Auenhammer et al. 2021, 2022; Florisson et al. 2022; Huber et al. 2022). Here, calibration indicates the iterative adjustment of model material properties until good agreement is found between modelled and expected behaviour. And, validation is the procedure where the ability of the model to predict the material behaviour is assessed using a set of chosen material properties.

The research conducted on XµCT aided FE modelling of wood is limited. Hachem et al. (2018) used the method to determine the thermal conductivity and diffusion coefficient of Norway spruce, whereas Badel and Perré (2002) used XµCT aided FE modelling to predict the elastic and hygroexpansion properties of oak. In Kamke et al. (2014) and Hammerquist and Nairn (2018), the method was used to study the mechanical behaviour of a phenol-formaldehyde adhesive bond line in wood through a combination of FE analysis and material point method. XµCT aided FE modelling was also found suitable to study wood composites. For example in Miettinen et al. (2016), and later in Fortino et al. (2017), the hygroexpansion coefficients of polylactic acid (PLA) reinforced birch pulp were estimated using this method. Verho et al. (2022) used the method to obtain the elastic moduli of wood composites in combination with a

homogenisation modelling strategy. XµCT aided FE modelling was also employed to study the mechanical behaviour of nanocellulose foams (Srinivasa 2017).

Currently, no clear integrated methodology for XuCT aided FE modelling of wood exists. Most research focuses on specific aspects of the XµCT aided FE procedure separately, such as image resolution, image segmentation or model meshing. This discontinuous approach undermines the compatibility between the steps that make up the XµCT aided FE process and complicates an efficient transfer of information between steps (Auenhammer et al. 2021; Keyak et al. 1990). Non-automated, i.e. manual procedures, can lead to realistic and specimen-specific estimation of material behaviour (Keyak et al. 1990), but can also create labourintensive processes and human-induced errors within and between each step (Auenhammer et al. 2021).

1.4 Research focus

The current paper proposes a methodology for XµCT aided FE modelling of wood and identifies the bottlenecks associated with this process. The methodology focuses on fast, accurate and repeatable data transfer with a high degree of automation by adopting commercial software. The proposed methodology is based on an extensive literature review. The literature review also attempts to present the state-of-the-art for XµCT aided FE modelling of wood. Studies with a focus on materials whose methods are equally applicable to wood, e.g. bone, foams and fibre composites, have also been included. A methodology is suggested in Section 2 and tested in detail in Florisson et al. (2023). A supporting background of the methodology is provided in Section 3 and the bottlenecks are discussed in Section 4.

2 Methodology

The suggested $X\mu CT$ aided FE methodology for wood is presented in Figure 1. The methodology was developed for heterogeneous microstructures such as wood, with a temperature and moisture dependent mechanical material behaviour. Based on the literature review, five different steps were identified, labelled source, experiment, image processing, model development, and product. Each step consists of several relevant sub-steps, which are presented in Figure 1 and supported by Table 1. A reference to the relevant sub-sections can be found in Table 1. Each step will be discussed in detailed in Section 3 and their bottlenecks in Section 4. Illustrations from literature are used throughout each section to support the text. In addition, results from a static state XµCT scan of compression wood obtained from a Norway spruce tree branch is used to clarify the specimen preparation, XµCT scanning, image reconstruction, segmentation and mesh step and some

of their bottlenecks. The main aim of the scan was to obtain a spatial and contrast resolution with a XµCT scanner high enough to identify the microstructure in the proposed steps.

The specimen preparation step is based - amongst other references - on the research conducted by Zauner (2014), whom expresses the importance of specimen geometry and conditioning on the quality of tomograms. The inclusion of a XµCT scanning and image-reconstruction step are straightforward, and their importance on image quality have been discussed in great detail since the arrival of the first lab-based scanner in the eighties. The material characterisation step is based on the extensive work by Lindgren (1988, 1992), whom created the foundation for the use of X-ray computed tomography in the Northern Swedish sawmills today. The segmentation step is identified as a standard procedure when geometry (complex geometry, geometry-based meshing) is an important aspect in the development of the FE model (Auenhammer et al. 2021). Since wood is a fibrous material and the orientation of the fibres largely contribute to the hygromechanical

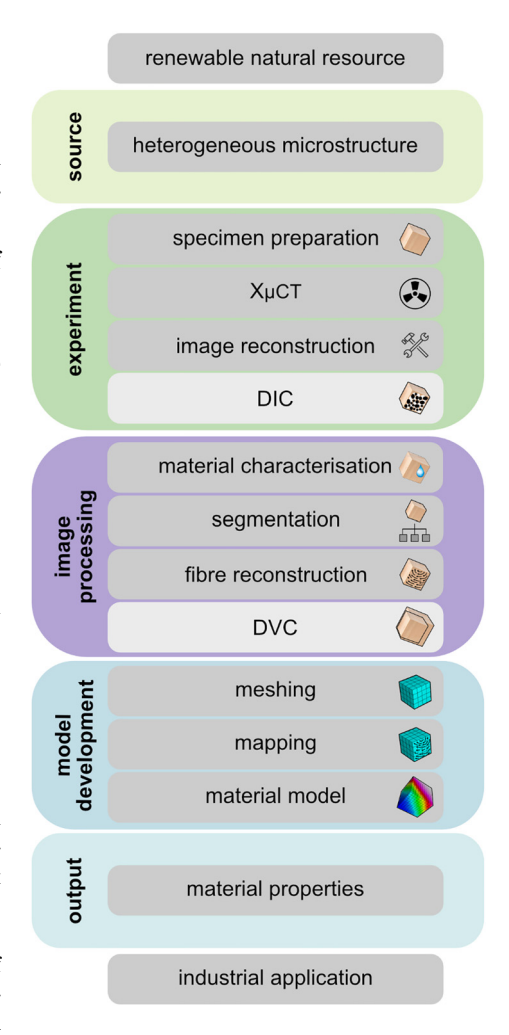


Figure 1: Suggested methodology for the microscopic lab-based computed tomography (XµCT) aided finite element modelling of wood, where DIC indicates digital image correlation (2D) and DVC indicates digital volume correlation (3D). The numbers indicate the subsections dealing with each step, where the underlying references of this review can be found.

Table 1: Short description of steps and sub-steps that make up the XµCT aided FE methodology for wood, including the main bottleneck and a reference to corresponding subsections.

	#	Step	Description	Main bottleneck
Experiment	3.1/4.1	Specimen preparation	Proper production of specimens to facilitate the subsequent steps of the XµCT aided FE process	Improper specimen design leads to image artefacts and low-contrast tomograms, which is problematic for image processing and model development
	3.2/4.2	XμCT scanning	Considerate selection of X μ CT scanner, experimental set-up and scanning parameters to optimise image quality and aid the overall X μ CT aided FE process	Spatial, contrast and temporal resolution and the occurrence of image artefacts are influenced by scanner, experimental set-up and scanning parameters. A lack of standardised <i>in-situ</i> test methods inhibits the extensive testing of wood
	3.3/4.3	Image reconstruction	Selection of ideal image-reconstruction algorithm to create tomograms	The image-reconstruction software is often provided by the producer of the scanner, leading to limited options and creating a rigid framework
Image processing	3.4/4.4	Material characterisation	Retrieval of information from tomograms using a direct or indirect relation between CT number and material characteristic	XμCT is not the best suitable method for the quantification of the linear attenuation coefficient
	3.5/4.5	Segmentation	Partitioning of digital images into multiple non-overlapping image segments (objects or phases) based on their greyscale level	The success of segmentation is largely dependent on the spatial and contrast resolution, and artefacts
	3.6/4.6	Fibre orientation	Retrieval of fibre orientation based on greyscale information in tomograms	Current algorithms cannot properly represent spiral grain, conical shape and annual ring curvature
Model development	3.7/4.7	Meshing	Selection of appropriate meshing techniques to develop the mesh and to check the quality of the mesh	Mesh quality checks are often omitted from the process, leading to inaccurate results
	3.8/4.6	Mapping	Assigning fibre orientation and material characteristic to the finite element mesh using appropriate interpolation techniques, where needed	Deviation between original and mapped results can arise due to the chosen mapping technique, leading to inaccurate results or convergence issues
	3.9/4.8	Modelling	Making a considerate choice in material model to simulate the desired material behaviour. This step determines the needed material properties	The design of the experimental step does not align with the image processing and modelling step, leading to inaccurate properties
Support	3.10/4.9	DIC and DVC	Supporting results from digital image correlation (DIC) and digital volume correlation (DVC) for model development, calibration and/or validation	DIC accuracy depends on the planeness of the studied surface, unless stereo cameras are used. DVC accuracy depends on spatial and contrast resolution of tomograms, and possible artefacts

behaviour of wood, the fibre orientation step is of essence. The importance is well illustrated by - for example - Huber et al. (2022). The meshing, mapping and modelling steps were identified in the work by Florisson (2022). Whereas, review articles, such as Roux et al. (2012), Maire and Withers (2014), Buljac et al. (2018), Withers et al. (2021), show the compatibility between methods such as X-ray computed tomography, finite element modelling, and DIC and DVC.

3 Literature review

3.1 Specimen preparation

The step specimen preparation focuses on the proper preparation of specimens to facilitate the subsequent steps of the XµCT aided FE process. The step necessitates decisions on specimen size, geometry and preparatory measures (conditioning, contrast agents) to minimise image artefacts

and optimise the spatial, contrast and temporal resolution of the tomogram. Size and geometry should accommodate the confined testing space associated with XµCT and prevent artefacts. Zauner (2014) shows that specimens used in compression tests requires horizontally symmetric surfaces to mount for loading in vertical direction, and that a cylindrical specimen shape can prevent tomographic artefacts and lead to more accurate predictions of compression stress. Since wood is a hygroscopic material, it will always try to establish an equilibrium with the outside environment. Correct environmental conditioning is therefore important to prevent artefacts (Florisson et al. 2022). In Figure 2, a rendered tomogram of the 1 mm³ cube of Norway spruce compression wood is presented. The tomogram was obtained with a Zeiss Xradia 510 Versa XuCT scanner. The cube was conditioned at room climate and scanned in a small sealed enclosure to prevent motion artefacts caused by

differences in relative humidity between room and scanner. In addition, the dimensions of the specimens were chosen to benefit the desired spatial resolution. Materials that have large differences in electron density will experience a relevant attenuation contrast (Withers et al. 2021). The attenuation coefficient increases with increasing atomic number due to the scattering of electrons and decreases with increasing X-ray energy (voltage, keV). In case of low contrast materials, the attenuation coefficient, and there with the contrast resolution, can be promoted by manipulating the chemical composition of materials by adding a contrast agent (e.g. Ching et al. 2018; Kamke et al. 2014; Kibleur et al. 2022a; Li et al. 2013; Paris et al. 2014, 2015; Withers et al. 2021).

3.2 XµCT scanning

The step $X\mu CT$ scanning is designed to select the type of $X\mu CT$ scanner, experiment and scanning parameters to optimise the quality of the images and aid the overall $X\mu CT$ aided FE process.

3.2.1 Computed tomography methods

The most popular categories of X μ CT are attenuation contrast and phase contrast imaging. The *attenuation contrast*, or absorption mode, is the most conventional mode to perform X μ CT (Derome et al. 2011; Salvo et al. 2003). This mode is founded on the Beer–Lambert law,

$$I = I_0 e^{-\sum_{i=1}^{n} \mu_i z_i}$$
 (1)

$$\mu_i = \frac{\ln\left(\frac{I_0}{I}\right)}{Z_i} \tag{2}$$

where, for an object comprising of multiple materials $(i=1\dots n)$ in the beam path, I is the intensity of the transmitted X-ray beam, I_0 is the intensity of the original X-ray beam, μ is the linear attenuation coefficient, and z is the thickness of the specimen. The law states that as the radiation moves through the material, it attenuates – or in other words – gradually loses flux intensity. *Phase contrast imaging* can be used for materials that attenuate similarly (Endrizzi 2018), making use of the phase shift that defines

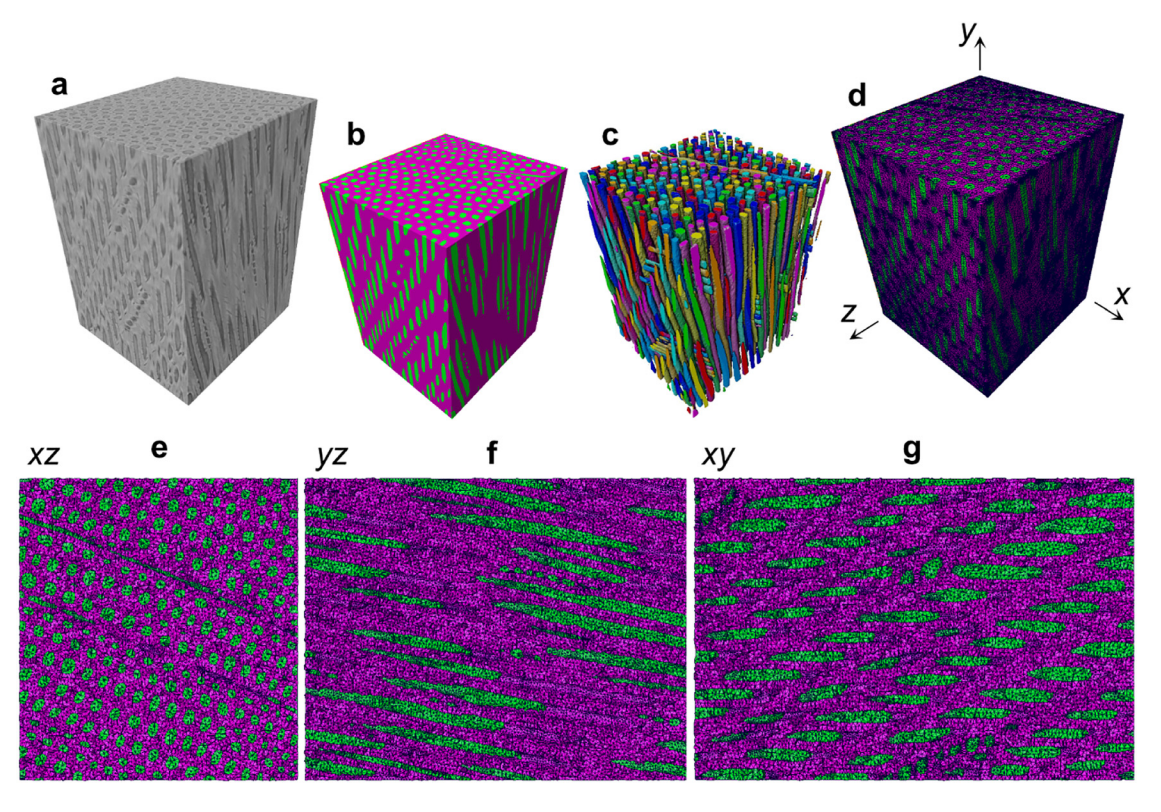


Figure 2: Example of segmented and meshed Norway spruce microstructure obtained with commercial software Avizo™: (a) render of microstructure, (b) segmented structure (green is lumen and purple is cell wall), (c) segmented lumen, (d) meshed geometry, (e) cross-section of meshed geometry in *xz*-plane, (f) cross-section of meshed geometry in *yz*-plane.

the refractive index. Since the detectors cannot measure a phase shift, this must be retrieved from the recorded patterns of the intensity, called phase retrieval. Patera et al. (2018b) used phase contrast imaging to study sorption and swelling behaviour of spruce. A deeper understanding of attenuation contrast and phase contrast imaging can be obtained by reading Maire and Withers (2014), Endrizzi (2018). Withers et al. (2021).

3.2.2 Experimental methods

Although the scanning times of XµCT are becoming shorter, the technique is most often used to image static state problems (Garcea et al. 2018; Zwanenburg et al. 2022). The method is also suitable to image dynamic processes that occur over a longer period of time. For dynamic processes that are not easily controlled, a post-mortem imaging approach can be maintained (Cordes et al. 2015). In such a case, tomograms will be acquired before and after the dynamic process has occurred. An interrupted in-situ approach can be taken for processes that can be easily controlled. The specimen will then be incrementally exposed to the dynamics process, with tomograms acquired between each interrupted step to create a time-lapse sequence of images during deformation and damage development (Cordes et al. 2015; Sisodia et al. 2019). Specimens can be tested using ex-situ and in-situ XµCT testing techniques (Buljac et al. 2018). Ex-situ testing means that the test rig is positioned outside of the scanner. In such a situation, the specimen is scanned prior, after and - in case of steady-state – during testing. In-situ testing indicates that the test rig is mounted inside the scanner (Buffiere et al. 2010). This requires a suitable specimen and test-rig size, and a test setup that does not affect the X-ray propagation (Zauner 2014). Wood is most often imaged using an ex-situ post-mortem approach, since environmental differences and time-dependent behaviour easily affect the material. Nevertheless, more recent studies have used an interrupted *in-situ* approach to investigate the swelling interactions of earlywood and latewood of spruce (Patera et al. 2018b) and water transport in medium-density fibre boards and oriented strand boards (Li et al. 2016). Uninterrupted in-situ testing of dynamic processes, such as moisture flow and elastic behaviour of wood, can be done using SRµCT (Couceiro et al. 2020; Forsberg 2008; Forsberg et al. 2008, 2010; Zauner 2014; Zauner et al. 2016). Fast imaging (around 0.3 s) in an uninterrupted in-situ setting can also be achieved using lab-based CT scanners, but usually at the costs of spatial resolution (Florisson et al. 2022; Garcea et al. 2018).

3.2.3 Scanning parameters

Identifying the appropriate scanning parameters begins with the needed spatial, contrast and temporal resolutions. which can be linked to the required object size, features of interest, and allowable dose of radiation (du Plessis et al. 2020). These decisions will determine the field of view (FOV) and the type of scanning: region of interest (ROI) or image stitching (Withers et al. 2021). The material type and the pathlength through the specimen determines the maximum X-ray energy of the beam. The maximum energy of the polychromatic spectrum is given in voltage (keV), where the current (mA) is the amount of charge generated by the X-ray tube per unit time. Voltage and current together amounts to power (Watt) produced by the scanner. A lower energy gives a higher attenuation contrast between different phases, but leads to lower transmission. A rule of thumb to determine the lowest energy given is a required transmission of >10-20 % through all projections (Withers et al. 2021). The last step is the choice of optical scanning parameters. In Section 4.2, a thorough overview of such parameters is given together with their influence on image quality.

The wood cube shown in Figure 2 was scanned using attenuation contrast imaging. The scanning involved a static state problem, since the purpose of the scanning was the investigation of the microstructure. The specimen geometry and scanning settings were chosen to obtain a spatial and contrast resolution that can capture the difference between lumen and cell wall assuming a low dense material. Before scanning an estimation of the size of these detectable objects were made and several test runs were performed to determine the ideal scanning parameters. The scanning settings that were used were a voltage of 50 kV, a power of 4.5 W, a source distance of 4.81 mm, an objective of 20x, a detector distance of 5.78 mm, a camera binning of 2, an exposure time of 0.7 s, and 2801 projections. This resulted in a spatial resolution of 0.61 um and a scan time of 1.5 h. No X-ray filters were needed to account for, for example beam hardening. But, to optimise the quality of the tomograms and account for potential ring artefacts, a low energy filter (LE1, Zeiss Xradia 510 Versa XµCT scanner) was used.

3.3 Image reconstruction

In the image reconstruction step, a mathematical procedure is selected to generate tomograms from the X-ray projections acquired at different angles around the scanned object. During image reconstruction, the attenuation coefficients (or phase decrements for phase contrast) are computed for different X-ray absorption paths obtained as a set of projections (Endrizzi 2018; Murphy and Haouimi 2022). The relationship between the projections is described by the Radon transform, which is an integral transform used to determine the one-dimensional profile of many projection: a sinogram (Withers et al. 2021). Reconstruction algorithms can be subdivided into analytic and iterative methods. The most common techniques available are the iterative algorithm without statistical modelling, the iterative algorithm with statistical modelling, the back projection, and the filtered back projection (Murphy and Haouimi 2022). The tomogram of the compression wood cube displayed in Figure 2 was created using a filtered back projection provided by the supplier of the scanner. The most recent development in image reconstruction is the adoption of machine learning methods. Machine learning methods can produce much better reconstructions than the conventional methods mentioned above. In addition, this category of reconstruction methods allows for a higher temporal resolution, due to shorter detector integration times and a possibility for viewer projections (Withers et al. 2021; Zwanenburg et al. 2022).

3.4 Material characterisation

3.4.1 CT number and density

The material characterisation step focuses on retrieving information from tomograms using a direct or indirect relation between CT number and material property (de Ridder et al. 2011; Maire and Withers 2014). This step is most often seen for attenuation contrast computed tomography. Each voxel in a CT scan can be labelled with a CT number (CT#) expressed in Hounsfield unit (HU). The HU is a dimensionless unit used to express the CT number in a standardised and convenient way (Greenway and Gaillard 2022), although other methods exists that do not rely on HU (de Ridder et al. 2011; Stubbs et al. 2020). The CT number can be obtained through a linear transformation of the linear attenuation coefficient.

$$CT# = \frac{\mu - \mu_{w}}{\mu_{w} - \mu_{a}} \cdot 1000$$
 (3)

where $\mu_{\rm w}$ is the attenuation coefficient of water (0 HU) and μ_a is the attenuation coefficient of air (-1000 HU). For wood, a proportionality exists between CT number and density, as well as density and moisture content (Hattori and Kanagawa 1985; Kanagawa and Hattori 1985; Lindgren 1985, 1991a, 1992). Lindgren (1992) showed that the relation between CT number and density is linear. Furthermore, Hansson and Cherepanova (2012) and Watanabe et al. (2012) used this relation to determine moisture content in wood using a tomogram of a moist wood piece and a tomogram of the same wood piece after oven-drying (dry-density image).

3.4.2 Density and material properties

The relationship between CT number and density can also be adopted to formulate other material properties (Keyak et al. 1997). Based on experiments, a linear correlation was obtained between the dry density of wood and elastic modulus (Kollmann and Côté 1968), hygroexpansion coefficient (Boutelie 1972), and diffusion coefficient (Sehlstedt-Persson 2001). Such correlations are not generic, though, and need to be validated for each situation. The justified relationships can then be used to obtain 3D information on material properties from tomograms (Florisson et al. 2022; Hartig et al. 2021; Huber et al. 2022). Such 3D profiles can be employed for situation specific simulations and a more realistic simulation of material behaviour (Keyak et al. 1997). For example, in Florisson et al. (2022), the dry-density profiles obtained with a medical CT scanner were used to quantify the diffusion and surface emission coefficients for Norway spruce for simulations of material behaviour during kiln drying. In Keyak et al. (1990), an empirical equation describing the relationship between elastic modulus and apparent density obtained from the grey levels in the reconstructed tomograms were used to simulate the stress fields in a human femur.

3.5 Segmentation

Image segmentation is the partitioning of digital images into multiple non-overlapping image segments (objects or phases) based on their greyscale level (Maire and Withers 2014; Withers et al. 2021). The voxels in the digital image are assigned a label, such that voxels with the same label share certain characteristics. The outcome of the image segmentation is a set of contours. Segmentation methods can be categorised as automatic, interactive (semi-automatic) or manual, depending on the degree of user involvement in performing the segmentation (Amrehn et al. 2019; Wang et al. 2016).

The objectives of the segmentation should be defined at the beginning of the XµCT aided FE process to decide on a correct segmentation method (Auenhammer et al. 2021). Manual, threshold-based, boundary-based and regiongrowing approaches are most prominently used (Withers et al. 2021). Manual segmentation can be advantageous or

even necessary for complex materials (Viceconti et al. 1998). Some popular automatic methods are the thresholding method (Otsu 1979), the watershed method (Beucher and Meyer 1993), and the deep-learning method (Akkus et al. 2017; Minaee et al. 2022; Seo et al. 2020). Figure 2 shows the segmented microstructure of a Norway spruce branch using manual (lasso, magic wand, brush) and thresholding techniques available in Avizo™. Image-processing techniques to fill holes, to discard small objects and remove unwanted voxel islands were also used to improve the segmentation. The thresholding method is a standard segmentation tool (Auenhammer et al. 2021). It uses the different greyscale levels of interesting objects within the tomogram to separate them from each other. The watershed method interprets the grevscale values of each voxel as altitudes. The morphological gradient of the original grey-scale image can be regarded as a topographic surface. The idea behind watershed algorithms is to compute watershed lines from this topographic image. The resulting catchment basins are the image partitions. A rapidly developing alternative to conventional methods is machine learning/deep learning for segmentation, which is most developed in medical CT image analysis (Litjens et al. 2017). However, Kibleur et al. (2022b) successfully implemented deep learning segmentation to obtain fibre bundles in medium-density fibreboards. To get a more thorough introduction on available segmentation methods, literature such as Russ and Neal (2016) can be consulted.

3.6 Fibre orientation

An important step in the XµCT aided FEM process for wood is defining the fibre orientation, and on a larger scale also annual ring curvature, spiral grain and conical shape. Two methods can be distinguished to reconstruct the fibre orientation based on tomograms. The first method relies on greyscale variation within an image to estimate the orthotropic material orientation. Within this method, techniques such as the Hough transformation for circles is commonly used to detect the location of the pith (Hansson and Cherepanova 2012; Huber et al. 2022) and the Gradient Structure Tensor to reconstruct the annual ring pattern and fibre deviation around knots (Hansson et al. 2016; Huber et al. 2022); see Figure 3. In addition to these methods, Ekevad (2004) used a moment of inertia tensor for spherical bodies to detect spiral grain and conical shape. The second method requires highresolution tomograms and uses techniques, such as Avizo™ fibre tracking, to find the centre line of individual fibres to provide insight into the exact fibre orientation, length and diameter. The method can reconstruct the fibre orientation around knots, as was seen in Hu et al. (2022).

3.7 Meshing

The two most popular meshing approaches in XuCT aided FE modelling are voxel-based and geometry-based (Auenhammer et al. 2021; Keyak et al. 1990; Lengsfeld et al. 1998; Viceconti et al. 1998). A representation of these approaches is given in Figure 4, together with a manually generated mesh. The principles are equally applicable to bone - as illustrated - and wood. The choice of meshing approach is often made based on how accurate the surface and boundary of a modelled object needs to be represented. In the *voxel-based approach* each element represents a voxel (Hartig et al. 2021). This results in a structured cubic lattice, which follows the main directions set by the Cartesian coordinate system linked to the tomogram. Often, an eightnode isoparametric brick element is used to construct the mesh, resulting in a stacked representation of the geometry. This can be computationally expensive. The most commonly used meshing approach is geometry-based meshing. Different techniques are reported in literature, such as the Delaunay triangulation, the marching cubes and the advancing front technique (Lobos et al. 2010). Compared to voxel-based, the geometry-based approach is more timeconsuming, but produces smooth surfaces. The approach can be subdivided in three steps: surface mesh reconstruction, mesh adaptation and volume mesh generation (Pagès et al. 2005; Lobos et al. 2010). The surface mesh is generated on the inner and outer contours of objects obtained with segmentation. Generally, a tetrahedral element is used, which is stiffer than a brick element but complies better with generating a shape. Commercial image-processing software commonly allow the creation of a surface and volume mesh after segmentation (Auenhammer et al. 2021; Pyrkosz et al. 2010). In Figure 5, the segmented microstructure of Norway spruce is meshed using the mesh tool provided by commercial software Avizo™. After construction, the surface mesh was coarsened to reduce computational time. The shown surface and volume mesh were adapted and improved (element reduction, element shape, intersecting elements) to suffice as a computational mesh and to increase numerical stability (Lobos et al. 2010; Pagès et al. 2005). This was done using a mesh quality check provided by Avizo™. A quality control of the volume mesh before simulation is highly recommended using adequate shape quality parameters (Auenhammer et al. 2021; Keyak et al. 1990; Pyrkosz et al. 2010; Viceconti et al. 1998). In the medical field, machine learning is making an entrance to aid in the generation of FE meshes from tomographic images (Pak et al. 2021). This method minimises computational complexity, improves mesh quality and speeds up the mesh generation (Pan et al. 2023).

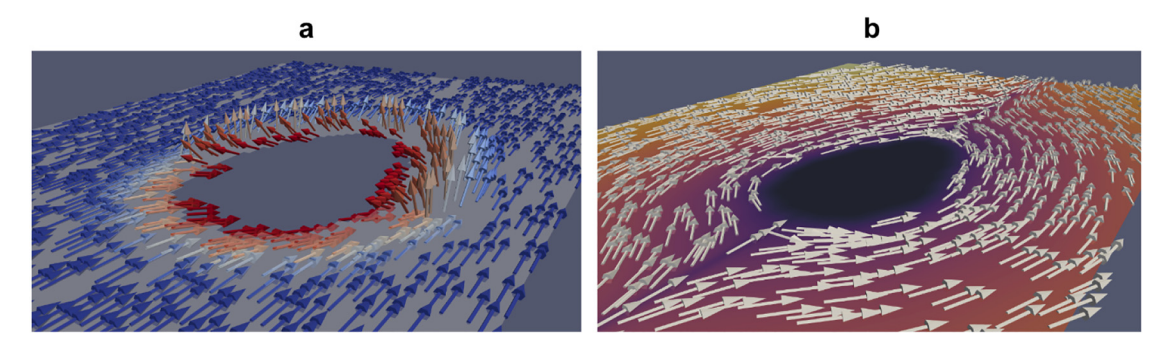


Figure 3: Example of reconstructed fibre orientation around knots based on tomograms from macro computed tomography: (a) diving vector field and (b) flow vector field (Huber et al. 2022, https://creativecommons.org/licenses/by/4.0/, changes were made to this illustration).

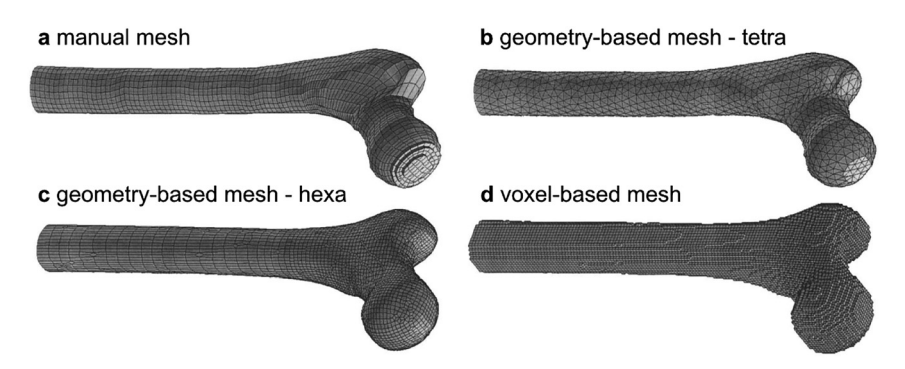


Figure 4: Example of key meshing methods, although visualised for a bone geometry: (a) manual meshing, (b) geometry-basedmeshing using a tetrahedral element, (c) geometry-based meshing using a hexahedral element, and (d) voxel-based meshing (Viceconti et al. 1998).

3.8 Mapping

During mapping, information from tomograms (e.g. fibre orientation, density, moisture content) is assigned to the FE mesh. A distinction can be made between an integrationpoint-wise, a node-wise or an element-wise approach (Auenhammer et al. 2021; Florisson et al. 2022). For example, mapping of density and moisture content data is done using a node-wise approach, which can be semi-automatic or automatic (Florisson et al. 2022; Huber et al. 2022). In the semi-automatic approach different programs are used to pre-process the data and to perform the mapping. Figure 6 shows the semi-automatic mapping of moisture content and dry density using a node-wise approach. During such mapping, the information at the voxel level is then transferred to the FE node level using a form of interpolation. Here, the mapping was performed in FE software Abaqus FEA®. The fibre or material orientation of wood can be mapped using an integration-point-wise or an element-wise approach (Auenhammer et al. 2021; Huber et al. 2022). In Huber et al. (2022), the material orientation of wood retrieved from tomograms was automatically mapped in a commercial FE software using the integration-point-wise approach. Auenhammer et al. (2021) discuss the mapping of fibre direction of composite materials using the elementwise approach. This approach requires the estimation of the centre of gravity for each element, after which the estimated fibre orientation at the voxel position closest to the centre of gravity is extracted and assigned as the local element orientation.

3.9 Material model

With the prediction of material properties as the goal of the XµCT aided FE process, the choice of material model dictates the amount and type of properties to be determined. It also influences the design of the experiment and the imageprocessing step. The majority of material models available for wood focus on the macro material level and upwards. In brief, the state-of-the-art mechanical models treat the hygromechanical (Huč et al. 2018), long-term (Bengtsson et al. 2022; Florisson et al. 2021b; Huč et al. 2020) and plastic behaviour (Oudjene and Khelifa 2009; Pech et al. 2021; Yu et al. 2022). Since wood is hygroscopic, also a strong interest lies with mass and heat transfer (Autengruber et al. 2020; Eitelberger and Hofstetter 2011; Florisson et al. 2020; Frandsen et al. 2007a, 2007b) and moisture-induced fracture in wood (Autengruber et al. 2021; Brandstätter et al. 2023). Some efforts have also been made on the micro material level, such as the hygroelastic behaviour of fibres (Persson 2000) and fracture behaviour of fibre clusters (Carlsson and

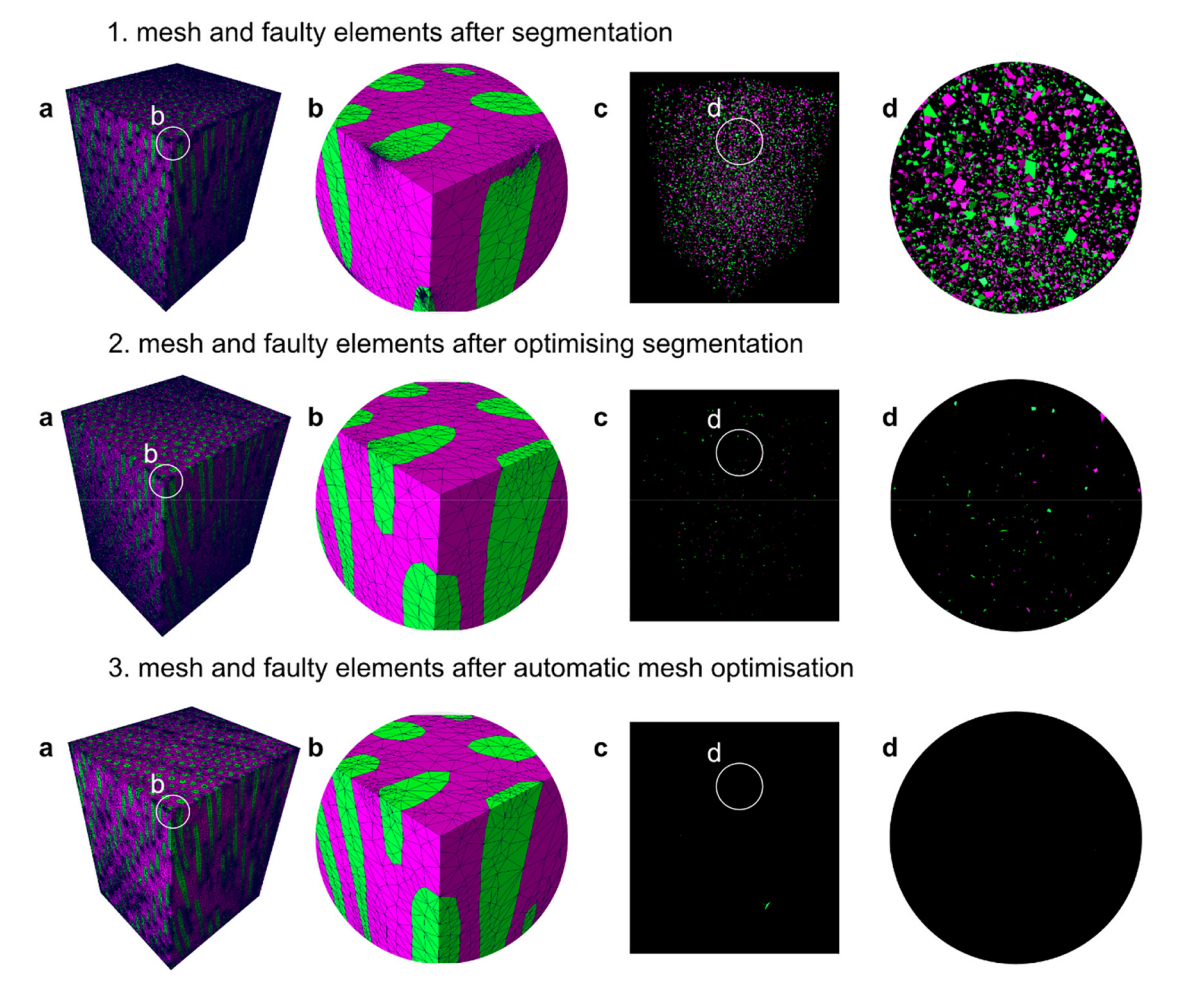


Figure 5: Example of mesh optimisation in three steps in commercial software Avizo™: (1) original mesh, (2) mesh after optimised segmentation and (3) mesh after quality check and automatic optimisation of bad tetras, where (a) is the meshed microstructure, (b) is a closeup of the microstructure, (c) are the identified bad tetras, and (d) is a closeup of the bad tetras.

Isaksson 2020). However, a thorough investigation into mechanosorption on micro material level using FEM is still lacking. Research has also been focussed on bridging the different hierarchical levels of mass transfer, elastic behaviour and large deformations using homogenisation methods (Eitelberger et al. 2011; Hofstetter et al. 2005; Holmberg et al. 1999; Zhong et al. 2021).

The material model step is also used to determine the level of detail of the FE model. For example, the model depends on the material level (cell wall, cell cluster, annual ring), the definition of properties (moisture, temperature and density-dependent), boundary conditions and initial simulation states. Therefore, a precise aim and objective should be set at the beginning of the process, and the model should be designed accordingly. Florisson et al. (2022) gives a good example where information from tomograms is incorporated into the details of an FE model to simulate moisture flow in boards of Norway spruce. This technique

was used to define the geometry, initial simulation states and diffusion and surface emission coefficients; see Figure 6. Another example is from Hartig et al. (2021), who showed detailed stress distribution in a moulded wood tube loaded in compression using a geometry and correlation between density and elastic moduli from tomographic data; see Figure 7. The results showed the clear effect of a density dependent elastic modulus on stress patterns.

Within the XµCT aided FE process, a direct or indirect approach can be adopted towards the prediction of material properties. The *direct* approach relies on other methods to aid in the prediction, such as digital volume correlation (DVC) (see Section 3.10) or other image-processing algorithms. For example in Stubbs et al. (2020), the properties were calibrated using data from compression tests. The indirect approach builds on the assumption that a relationship exists between the attenuation coefficient, density and the material property of interest (Boutelje 1972; Hartig

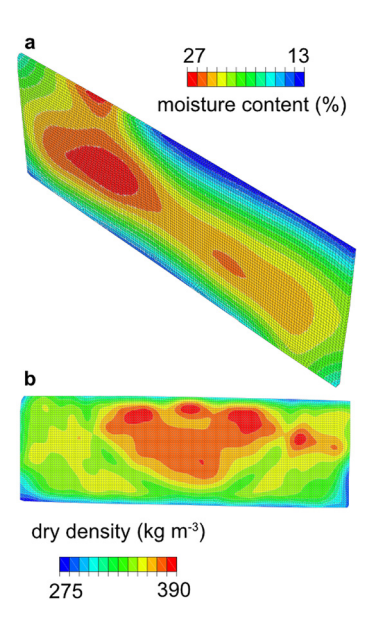


Figure 6: Example of mapped material characteristics on model geometry obtained from computed tomography data: (a) moisture content at the start of the simulation and (b) dry density profile used by the finite element program to describe diffusion and surface emission coefficient (Florisson et al. 2022, https://creativecommons.org/licenses/by/4.0/, changes were made to this illustration).

et al. 2021; Lindgren 1992; Taddei et al. 2004). For wood, experimental investigations have shown that a linear correlation exists between density and elastic modulus

(Kollmann and Côté 1968), hygroexpansion coefficient (Boutelje 1972), and diffusion coefficient (Sehlstedt-Persson 2001). The indirect approach can use pre-existing assumptions of such relationships or require a calibration as suggested for the direct approach. However, the indirect approach adequately takes into account variation of material and therefore leads to situation specific predictions of material behaviour, such as the stress distributions during static loading (Hartig et al. 2021; Huber et al. 2022; Keyak et al. 1990) or moisture distributions within a timber board during kiln drying (Florisson et al. 2022).

3.10 DIC and DVC

Digital image correlation (DIC) and DVC are popular imageprocessing techniques that are often used in conjunction with X μ CT (Buljac et al. 2018; Maire and Withers 2014; Roux et al. 2012). DIC is a contactless spatial measurement technique to obtain the deformation or strain field of a surface of an object (Zink et al. 1995), which can be used to validate the numerical results from X μ CT aided FE modelling (Hartig et al. 2021; Keunecke et al. 2012). DVC is an extension of the more conventional DIC and can estimate the threedimensional deformation or strain field of an object based on a reference image (fixed image) and its deformed state (moving image) (Bay et al. 1999). The method can be used to

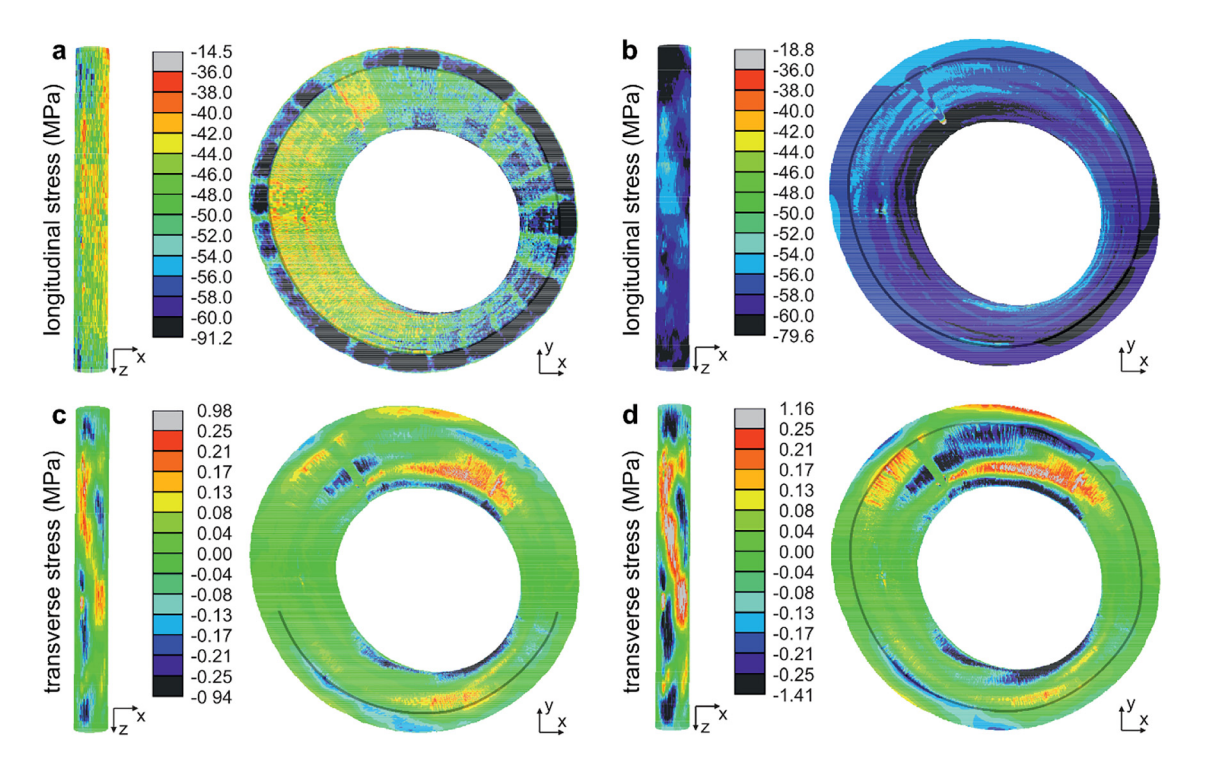


Figure 7: Example of simulated stress differences by integrating the variation in density into a finite element model: (a, c) longitudinal and transverse stress distributions for finite element simulations of a wood tube with varying elastic properties through computed tomography (b, d) and constant elastic properties (Hartig et al. 2021).

calibrate $X\mu$ CT aided FE models (Buljac et al. 2018; Forsberg et al. 2010; Hild et al. 2016) or as a Dirichlet boundary condition (Leclerc et al. 2010).

The most popular DVC approaches can be categorised as local or global (Buljac et al. 2018; Madi et al. 2013; van Dijk et al. 2019). The ROI in local DVC is subdivided into small volumes that are independently registered (Bay et al. 1999), where image registration is the process of transforming an image of an object into the same coordinate system. Local DVC has been successfully applied to analyse the elastic behaviour of wood (Forsberg et al. 2008, 2010; Tran et al. 2013); see Figure 8. Global DVC uses global image registration and relies on a linear inversion problem (Madi et al. 2013). The analysis results in a continuous displacement field. Global image registration uses a single equation to map the entire image. Examples of global registration methods are affine registration and non-rigid (or elastic) registration. Affine registration includes translation, rotation and scaling, whereas non-rigid registration can locally warp the image by using e.g., B-splines (Madi et al. 2013; Patera et al. 2018a). Global DVC has been successfully applied to analyse the swelling behaviour of spruce (Patera et al. 2018a) and medium-density fibreboards (Kibleur et al. 2022b).

4 Current bottlenecks

In the following subsections, a summary of expected bottlenecks associated with the $X\mu CT$ aided FE process of wood are outlined. A focus is put on bottlenecks that influence the automation of the process and errors within certain steps that can directly or indirectly affect the quality of later steps.

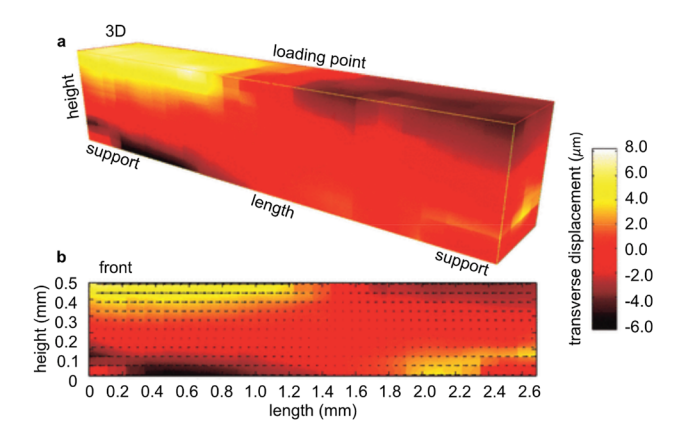


Figure 8: Example of digital volume correlation used to obtain displacement fields during bending of a piece of wood: (a) 3D representation of the transverse displacement and (b) front view of the same displacement field (Forsberg et al. 2008).

If these impediments could be alleviated, a momentous increase in efficiency is expected in solving scientific and engineering problems with CT and FEM. Throughout the section, mention is made of different relevant specimenbased, physics-based, and hardware-based artefacts (Cuete and Murphy 2022). A proper mitigation of artefacts within the $\text{X}\mu\text{CT}$ aided FE process is important, since they complicate material characterisation, segmentation, image processing and model development. A full overview of possible $\text{X}\mu\text{CT}$ image artefacts can be found e.g. in Hsieh (2015).

4.1 Specimen preparation

4.1.1 Artefacts

The importance of specimen preparation to reduce image artefacts was primarily addressed by Zauner (2014). The research stated that fewer disturbances were achieved during scanning by using a rotationally symmetric design for wood specimens. This shape led to a more accurate prediction of stress caused by compression. In this section the focus is on specimen-based artefacts and hardwarebased artefacts that can arise due to specimen design. A mentionable hardware-based artefact, known as out-offield, is caused by the specimen being too large for the field of view (FOV) (Zauner 2014). This artefact leads to increased or decreased density values and can lead to streaking. Therefore, the specimen should fill a high percentage of the FOV, without parts being outside of the FOV. Withers et al. (2021) mentions that the consequences of this artefact are minor (slight shifts in contrast) and that the diameter of the specimen can be ten times larger than the FOV. Motion artefacts can arise when the specimen experiences dimensional changes during scanning larger than the voxel size due to creep or changes in temperature or relative humidity. The artefact presents itself as blurs, streaks or shades (Kamke et al. 2014). In ex-situ testing, this artefact arises due to environmental differences between storage and scanner and can be mitigated by proper climatisation of the specimens and coverage of specimens using plastic during scanning. With in-situ testing, motion artefacts can be prevented by using a built-in climate chamber inside the scanner. This testing method also requires fewer specimens and adds to the validity of observed features by enabling continuous measurements (Buffiere et al. 2010; Garcea et al. 2018). Additionally, de Schryver et al. (2018) added to this solution a motion compensated reconstruction method for the in-situ analysis of dynamic processes using DVC.

4.1.2 Contrast enhancement

Another challenge in specimen preparation is contrast sensitivity, which indicates to what extend small nuances in attenuation coefficient can be detected. Materials with similar atomic number tend to produce limited absorption contrast (Withers et al. 2021). Low-contrast materials can lead to difficulties to distinguish small and closely spaced features, which can lead to challenges during segmentation and DVC (Roux et al. 2012). Unfortunately, the microstructure of natural materials is difficult to modify. In the case of engineered materials, this challenge can be overcome by enhancing the attenuation coefficient of the material that overlaps with other materials. Such contrast agents are highly attenuating particles, gasses or stains (Withers et al. 2021). In Li et al. (2013), the attenuation difference between wood and water was increased by using water doped with caesium chloride as a contrast agent. In addition, commercial wood adhesives can be tagged with iodine to improve the contrast between glue and wood (Ching et al. 2018; Kamke et al. 2014; Paris et al. 2014, 2015). In Kibleur et al. (2022a), the resin in wood fibreboards was doped with Potassium bromide to enhance the attenuation coefficient, where in Paris et al. (2015), iodinated phenol formaldehyde resin was used to enhance the contrast between bond line and wood; see Figure 9.

4.2 XµCT scanning

4.2.1 Image quality

Image quality evaluation and achieving a sufficient image quality are essential for an adequate image analysis (du Plessis et al. 2020). However, a standardised image quality metric to stimulate reproducible results is still lacking, which introduces reliability issues caused by instrument type, hardware and software used for image analysis, scanning environment and skill and experience level of operators (du Plessis et al. 2020; Withers et al. 2021; Zwanenburg et al. 2022). In Table 2 a summary is given of variables influencing the quality of scanning.

A general challenge with XµCT scanning is the wide choice of power (current, voltage), exposure time and filter to enhance the spatial, contrast and temporal resolution (Zwanenburg et al. 2022). The selected spatial resolution must be significantly smaller than the size of the expected features or their separation (Withers et al. 2021). Despite such an assumption, small features (cracks, defects) can still be difficult to detect. Power is a limiting factor when it comes to spatial resolution, since a larger spot size increases the

penumbra effect (see next subsection) (Zwanenburg et al. 2022). The focal spot size is the area of the X-ray tube where the X-ray radiation is emitted to the specimen. A higher power increases the intensity of the electron beam, the heat in the focal point and the focal spot size. A smaller spot size can be accomplished with a longer exposure time, which is proportional to the number of photons detected per projection. A longer exposure time leads to a lower temporal resolution, but brighter images with lower noise.

The contrast resolution of a tomogram is affected by both voltage and current. High voltages are not suitable for a low-density material such as wood, since the X-rays will move through the material without much attenuation, producing a low contrast image. High currents will result in a brighter image and lower noise, i.e. random variations in voxel values, but a too high current gives saturated images. Image noise affects image reconstruction and needs to be managed during scanning or removed before segmentation using a median or other filter (Withers et al. 2021). Because the polychromatic beam is far from uniform, and the detectors show pixel-to-pixel variation in sensitivity, a projection must be acquired without the specimen in the FOV to compensate for these variations during reconstruction. This is called a flat field correction (Seibert et al. 1998). Filters can be used to increase the mean energy of the spectrum by absorbing the lower energy X-rays, which will result in an improved penetration of the filtered spectrum.

4.2.2 Artefacts

A general challenge in the XµCT aided FE process is the presence of artefacts in tomograms. In this section hardware-based artefacts are discussed, which arise as part of the XµCT scanning procedure. The focal spot size and an increasing spot size, can contribute to the penumbra effect (Brunke et al. 2008; Kueh et al. 2016). This effect is observed as light (cell-wall side) and dark (lumen side) shadows in the region where air and cell wall intersect, and results in poorly defined edges (Kamke et al. 2014). Thermal drift of the X-ray emission point can lead to artificial motion and magnification changes in projections (Wang et al. 2017). This is caused by a change in source-object distance and object-detector distance during scanning due to generated heat in the X-ray tube (Limodin et al. 2011; Wang et al. 2017). A proper system warm-up or correction using a reference scan taken at the start can prevent this phenomenon from occurring. The detector can be prone to defective or uneven pixel response, which can result in ring artefacts (du Plessis et al. 2020). This artefact presents itself as circular rings around the rotational axis, which can be mistaken for pores (du Plessis et al. 2020). The long

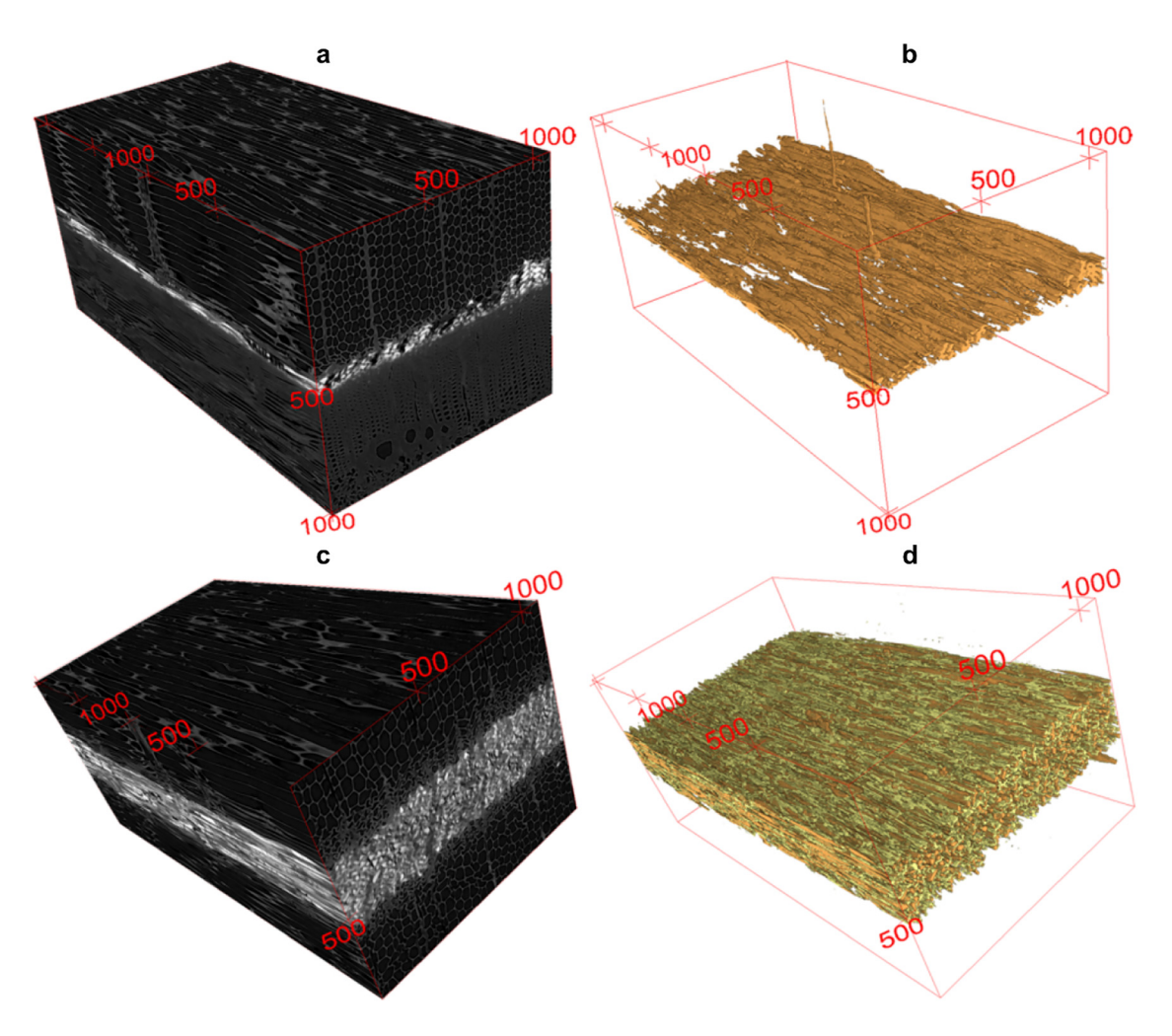


Figure 9: Example of contrast enhancement in XμCT of wood-based materials: iodinated phenol formaldehyde resin bond lines, (a) glued Douglas fir, (b) segmented bond line Douglas fir, (c) glued loblolly pine, and (d) segmented bond line loblolly pine (Paris et al. 2015).

Table 2: Variables affecting the uncertainty of computed tomography measurements (du Plessis et al. 2020; Withers et al. 2021; Zwanenburg et al. 2022)

Category	Examples of influencing variables
Computed tomography system	X-ray source, detector, axes, hardware filtering, scan mode, system type and other components of the scanner
Application	Object materials and geometry, fixturing, scanning parameters, reconstruction parameters, other settings
Analysis	Algorithms and software for reconstruction, segmentation and data analysis
Environment	Temperature, humidity, vibrations, other ambient conditions
Operator	Choices made by operator on measurement procedure and implementation, such as scan time, voltage change,
	mounting errors, binning, averaging, number of projections

scanning time of X μ CT compared to SR μ CT can lead to motion artefacts in the reconstructed tomograms (Roux et al. 2012). This makes it difficult to use X μ CT to conduct real time monitoring of phenomena such as crack initiation and propagation, abrupt material failure, viscoelastic behaviour, hygromechanical behaviour and diffusion

processes (Auenhammer et al. 2021; Cordes et al. 2015; Forsberg et al. 2008; Pyrkosz et al. 2010). Mechanical instability of setup and specimen due to the fixture or mounting can also lead to blurring and can be induced by an offset of the rotation centre (du Plessis et al. 2020; Withers et al. 2021). The polychromatic beam used in $X\mu$ CT

can lead to beam hardening, which increases the apparent density towards the edges of a tomogram (Bryant et al. 2012). Maire and Withers (2014) showed that this impairs global thresholding of bone based on a single greyscale value.

4.2.3 Data amount

A general challenge with XµCT is the enormous amount of data generated during scanning to obtain high temporal and spatial resolutions. This requires adequate transportation of data and storage space (Withers et al. 2021).

4.3 Image reconstruction

4.3.1 Projections

Image reconstruction is often performed using software provided by the machine supplier (Zwanenburg et al. 2022), as was seen in Figure 2, which can lead to unilateral and possibly inconsiderate choices in reconstruction approach. In XµCT, the reconstruction time is a limiting factor in fast scanning (Zwanenburg et al. 2022), where machine learning methods can reduce detector integration times and decrease the number of projections (Withers et al. 2021). In a traditional setting, the minimum amount of projections that is recommended for a quality image is $q\pi/2$, where q is the number of pixels across the diameter of the object (Withers et al. 2021; Zwanenburg et al. 2022). Going below the recommended amount of projections or applying non-uniform projections leads to noisy images with artefacts, although a slight reduction in projections is possible.

4.3.2 Artefacts

Beam hardening correction is often provided by reconstruction software of the machine supplier. However, an increase in correction factor often reduces the contrast in different parts of the tomogram (du Plessis et al. 2020; Wang et al. 2017).

4.4 Material characterisation

XµCT is not the most suitable method for the quantification of the linear attenuation coefficient and therewith the CT number. Such quantification would require a well-defined source, a monochromatic beam and a simple attenuation application (Maire and Withers 2014; Stubbs et al. 2020). In contrast, lab-based scanners produce a polychromatic beam

(white radiation) and scattered photons, while the detector is prone to defective or uneven pixel response (ring artefacts) and can charge bleeding (full pixels) (Maire and Withers 2014). The CT number is known to be energy-dependent, which is problematic when using a polychromatic beam (Bryant et al. 2012). Therefore, when using XµCT to determine density, the proposed sample set needs to be scanned under the same conditions as the unknown specimen. In this realm, the established relationship is only valid for the specific scanner and setting (de Ridder et al. 2011; Lindgren 1991b). When evaluating the density value, it is important to determine whether the observed greyscale fluctuation is due to a change in density, composition of material or imaging artefacts (Maire and Withers 2014).

4.5 Segmentation

Segmentation can be a bottleneck in an automated XµCT aided FE modelling process (Auenhammer et al. 2021; Keyak et al. 1990). According to Auenhammer et al. (2021), after p and h mesh refinement (higher degree of nodes and finer mesh, respectively), the error between segmentation, meshing, modelling and calibration is due to the segmentation process.

4.5.1 Image quality

The success of the segmentation process is closely linked to the spatial and contrast resolution of the tomogram and existing artefacts. Limited spatial and contrast resolution causes contours of closely positioned objects to combine. This was for example seen in tomograms of the acetabulum and the femoral head when scanning bone (Keyak et al. 1990). Small adjustments made in segmentation thresholding can highlight features that are actually noise or can join objects that are actually gaps (Withers et al. 2021). Therefore, decisions made in previous steps of the XµCT aided FE process directly influence the segmentation step. Pyrkosz et al. (2010) mentions that most standard segmentation methods that rely on the density variation within tomograms are unsuitable for wood, since the density variation of sapwood, heartwood, latewood, earlywood and transition wood largely overlap. Manual segmentation methods can be more suitable in such situations, but are time consuming, non-repeatable, a source of human error, and compromises the automation of the XµCT aided FE process. Figure 10 visualises this challenge for the 1 mm³ cube of Norway spruce branch wood, where the lumen is segmented from the cell wall. The figure shows that automated segmentation methods do not hold due to the overlap

of density values, and manual tools are needed for a precise segmentation.

4.5.2 Artefacts

A general concern of the segmentation step is the presence of image artefacts. An important physics-based artefact is beam hardening. Maire and Withers (2014) showed that for bone this artefact prohibits the use of global thresholding based on a single greyscale value. An artefact particularly interesting for wood is the partial volume averaging effect that occurs when two or more phases with different densities are encompassed at the same voxel (Cuete and Murphy 2022). This produces an average attenuation coefficient of those phases, which challenges the segmentation process (Hartig et al. 2021; Pyrkosz et al. 2010). For wood, this artefact can occur at the surface of a specimen, where a voxel can contain both air and wood (Huber et al. 2022), or when scanning thin adhesive coatings in wood fibre materials (Kibleur et al. 2022a). The latter can be overcome with lab-based dual-energy CT.

4.6 Fibre orientation and mapping

A mapping accuracy check should be performed for both material orientation and material properties (Florisson et al. 2022; Stubbs et al. 2020). Mapping deviations can influence the FE results and therefore the determined material properties. For example, misalignment of fibres during mapping can lead to stiffness reduction (Auenhammer et al. 2021; Huber et al. 2022). This can affect the FE analysis convergence rate and the stress and strain output. Mapping information onto a new set of coordinates can also lead to errors depending on the interpolation method. Florisson et al. (2022) showed a small deviation between the original and mapped moisture content data. A linear interpolation was performed in commercial FE software Abagus FEA[®].

4.7 Meshing

The quality of the FE mesh can be assessed based on computational weight (total operator time and total CPU time) and computational accuracy (in comparison with an analytical solution or experimental results) (Lobos et al. 2010). For instance, a manually created mesh requires a long operator time compared to a voxel-based mesh or a geometry-based mesh, but can result in efficient and accurate models. The adequacy of a mesh generated from tomograms is often not verified (Keyak et al. 1990; Viceconti et al. 1998), since it is a very time consuming process. A mesh quality check is especially important when handling complex geometries, and is needed particularly to omit elements with severe shape distortions and large aspect ratios (Lobos et al. 2010; Song et al. 2017). These issues are visualised in Figure 11, together with an indication of the bounded surface deviation error. This is the gap between the mesh and the analytical surface, and needs to be considered when an accurate representation of surface is required (Pagès et al. 2005).

4.7.1 Voxel-based mesh

Voxel-based meshing is an easy and fast way to generate a 3D mesh from tomograms (Viceconti et al. 1998). The method is insensitive to complex geometries and low

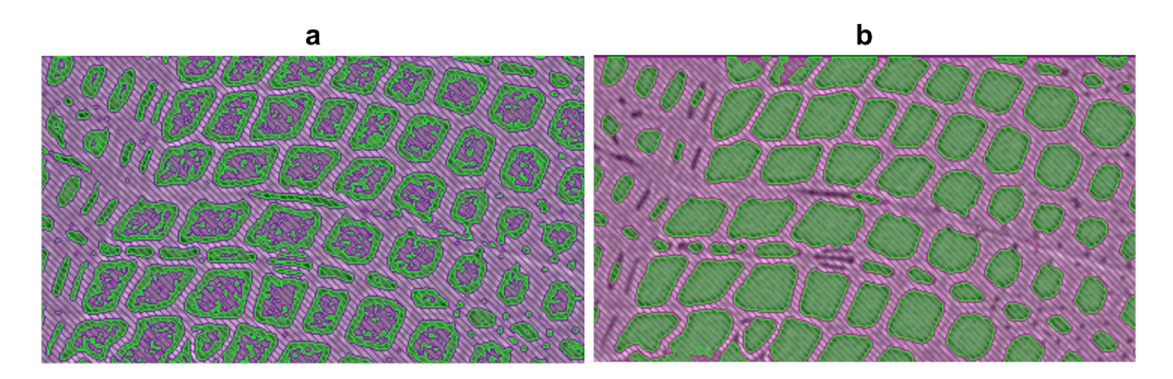


Figure 10: Example of segmentation of the lumen that make up the microstructure of Norway spruce using commercial software Avizo™: (a) segmentation based on only thresholding and (b) segmentation based on multiple segmentation methods such as thresholding and manual (lasso, magic wand, brush) and image-processing techniques to fill holes, discard small objects and remove voxel islands.

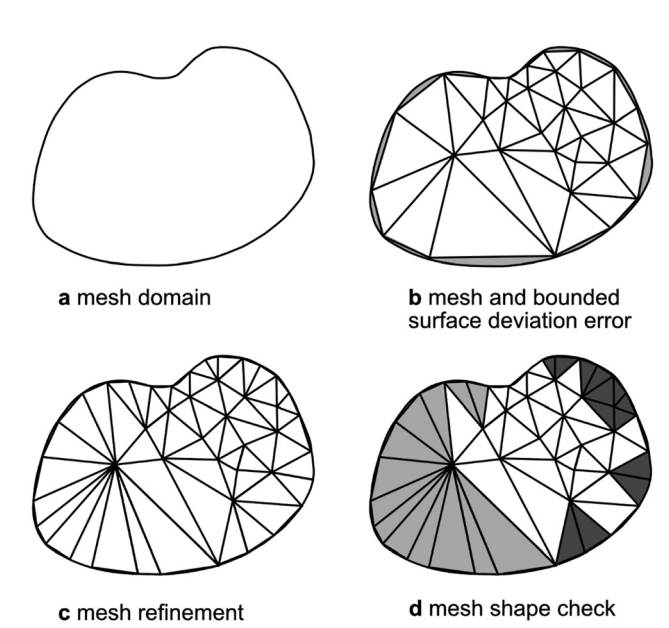


Figure 11: Example of mesh adequacy issues: (a) the mesh domain, (b) the meshed domain with a visible bounded surface deviation error (light grey areas), (c) mesh refinement to minimise the bounded surface deviation error, and (d) a mesh shape check of the added elements during mesh refinement (light is bad shape, dark is good shape) (Lobos et al. 2010).

image resolution, but cannot give a precise representation of geometry and boundaries between phases. This mesh type should be avoided when analysing surface phenomena, such as fracture initiation and stress-strain concentrations. A voxel-based mesh needs a high level of mesh refinement for accurate results, which leads to large computational efforts and long operator times (Song et al. 2017; Viceconti et al. 1998). It was mentioned by Marks and Gardner (1993) that the jagged pattern of the inner and outer surfaces can cause for numerical problems, since the unsmoothed surface can result in convergence issues for elements with sharp discontinuities.

4.7.2 Geometry-based mesh

The general challenges that effect the segmentation step also influence geometry-based meshing (Auenhammer et al. 2021), such as complex geometries in combination with low image quality (resolution and artefacts). The complexity of generated surfaces meshes also forms a bottleneck, especially in an automated XµCT aided FE process (Auenhammer et al. 2021), since it requires a mesh simplification to prevent mesh quality issues and mesh penetration. In Figure 12, mesh clusters are displayed, which were obtained for the example of the compression wood specimen, and occur when thin segmented objects lie beneath the surface of a ROI. These clusters are difficult to remove and require adjustments of the segmentation. In Figure 12, it can be seen how the segmentation is levelled to the surface, which removes the unwanted mesh cluster. A geometry-based mesh is often constructed from tetrahedral elements, which are computationally costly.

4.8 Material model

A general challenge in the material model step is an insufficient correlation between experimental design, image processing and material model, leading to an inaccurate prediction of the material parameters. A proper inventory is needed of required variables, such as material level, level of modelling detail, selection of material properties, physical phenomena influencing the observed system (temperature, relative humidity) and studied physical phenomena. Some physical phenomena are difficult to study experimentally, such as mechanosorption, which always occurs in combination with an elastic, creep and hygroexpansion component, and requires a well-designed experimental methodology (Florisson et al. 2021a). It should also be stated that a description of the hygromechanical behaviour of wood needs a large set of material properties, which necessitates many experiments (Huč et al. 2018, 2020). Other phenomena need a different level of modelling detail dependent on the material level. In Florisson et al. (2022), the diffusion and surface emission coefficient were determined using macroscopic tomograms of the kiln-drying process of wood. A nonlinear transient moisture flow analysis was made using a single Fickian equation, and moisture, temperature and density dependent material properties. However, in Frandsen et al. (2007b), a similar analysis was made, but using a multi-Fickian approach. This approach makes a distinction between diffusion in the cell wall and cell lumen, allowing for the incorporation of sorption hysteresis into the simulation. This is not possible using a single Fickian approach. In Section 3.8, it was also noted that many material models have been developed and validated on the macro material level, which poses a question whether such models still hold when describing the behaviour of the cell wall or an individual fibre. For example, one of the well-known material models to describe mechanosorption has only been applied to simulate wood behaviour on meso to timber scale (Salin 1992).

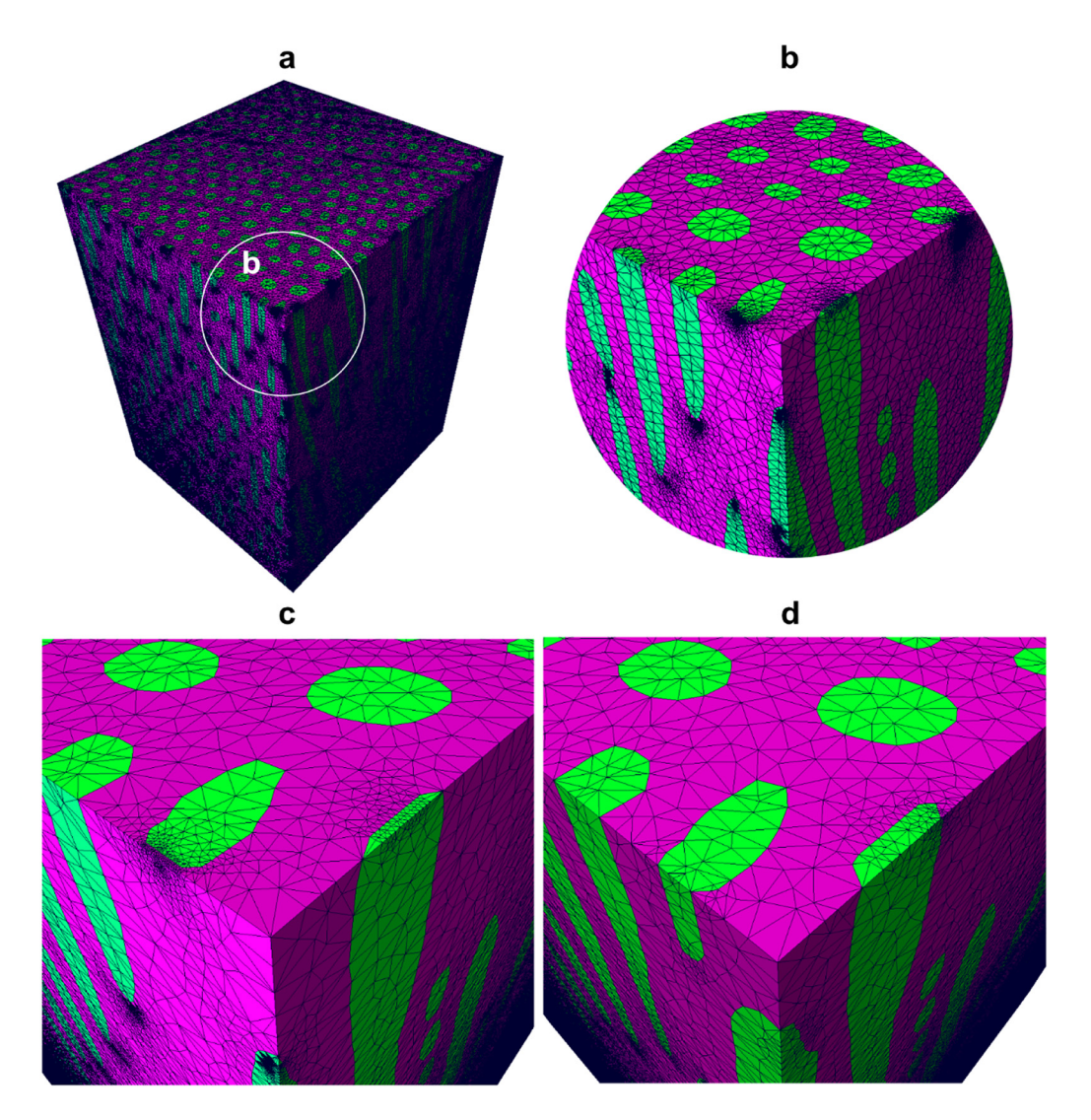


Figure 12: Example of surface mesh issues caused by thin objects produced during segmentation: (a) surface mesh for a Norway spruce microstructure using geometry-based meshing approach in commercial software Avizo™, (b) close-up, (c) a thin object underneath the surface and a thin object at the surface, and (d) issues resolved by increasing the size of the objects.

4.9 DIC and DVC

4.9.1 Image quality DVC

The accuracy of a 3D imaging technique based on *DVC* largely depends on image resolution (spatial and contrast) and algorithm quality (Buljac et al. 2018; Leclerc et al. 2012; Wang et al. 2017). This section will focus on the first component. For a thorough review on DVC and its challenges, Buljac et al. (2018) can be consulted. DVC is largely dependent on spatial contrast, where insufficient voxel size can make it difficult to detect important features, such as crack openings (Roux et al. 2012). In addition, the images need sufficient contrast to represent the microstructure, since the algorithm needs a recognisable random pattern to

converge (Roux et al. 2012). DVC can pose challenges when applied on materials without significant density gradients and with noticeable artefacts. Softwoods e.g. have a rather uniform longitudinal material direction, which can form a risk for DVC decorrelation (Forsberg et al. 2010). This can be solved by using tomograms with sufficient spatial and contrast resolution to emphasize the bordered piths. This approach led to good DVC results for Norway spruce beams tested in bending, without the need for contrast-enhancing particles (Forsberg 2008; Forsberg et al. 2008, 2010). A general limitation of DVC is the handling of large data files (Roux et al. 2012). Here, commercial software, such as Avizo™ (Thermo Fisher Scientific 2022), can aid in the management of such large datasets by providing efficient data-processing tools and efficient GPU implementation.

4.9.2 Artefacts DVC

DVC decorrelation also arises from noise and artefacts in tomograms, such as ring artefacts, beam hardening and motion artefacts (Buljac et al. 2018; Limodin et al. 2011; Roux et al. 2012). Artefacts can lead to spurious DVC results, especially when tomograms lack contrast (Buljac et al. 2018). Modern XµCT scanners come with tools to numerically filter artefacts from tomograms, such as beam hardening reduction (Wang et al. 2017). As previously mentioned, such filters can reduce density gradients. Thermal drift of the X-ray emission point can also negatively affect the DVC analysis (Limodin et al. 2011; Wang et al. 2017), which leads to displacement and strain errors. This error increases with scan duration, but can be minimised with a warm-up scan (Wang et al. 2017). Rotational and translational misalignment of specimens due to ex-situ testing or loading procedures create a general source of error in DVC (Forsberg et al. 2010). Such misalignment can often be manually corrected during reconstruction. Another challenge with DVC and exsitu testing is the intensity differences in the background between tomograms, which can lead to large correlation errors (Buljac et al. 2018).

4.9.3 DIC

Image resolution for a 2D imaging techniques such as DIC is less challenging. The homogeneity, pattern correlation length and image contrast can be enhanced by adjusting the signature speckle pattern (Buljac et al. 2018). A general difficulty with surface imaging methods, such as DIC, is the production of plane surfaces without introducing artefacts by machining tools (Forsberg et al. 2008). The surface should also remain plane after deformation of the specimen. Most modern DIC systems come with two cameras to detect out-of-plane deformations, which can be considered during post-processing.

5 Concluding remarks

The proposed XµCT aided FE methodology for wood covers the process from specimen preparation to material property estimation. The literature review gives underlying information for each step that make up this process. The main bottlenecks that can occur between and within each step have been identified. The review covers research also for other materials (e.g. bone, concrete, fibre composites, foams and plastics) whose results are applicable for wood materials. Conversely, the XµCT aided FE methodology is equally applicable for these materials, disregarding the specificities of wood materials.

A general conclusion that can be drawn from the literature review is that the methodology can assists in a considerate design and execution of the XµCT aided FE process for wood. This means that the best modelling results are obtained with the definition of a clear aim and objective at the beginning of the XµCT aided FE process. This should steer towards an experimental step that is designed and executed to benefit the image processing and model development step. The tomograms should be of sufficient quality (see spatial, contrast and temporal resolution, and lack of artefacts) to be able to perform the material characterisation, segmentation, fibre reconstruction, DVC and meshing step.

There are a couple of current bottlenecks for wood applications that are pressing to resolve in short-term. The absence of a standardised method for in-situ testing of wood prohibits the extensive testing of the hygromechanical behaviour using XµCT. Also, the prevalent traditional segmentation and meshing techniques prevent an automated XµCT aided FE process for wood. Therefore, a combination of deep-learning segmentation methods combined with geometry-based meshing is suggested to stimulate this development. As a last note, it can be mentioned that simple and effective algorithms to generate the orthotropic material orientation of wood from tomograms, including spiral grain, conical shape, annual ring curvature, and grain deviation around knots would be very useful.

Acknowledgements: The authors thank Fredrik Forsberg and Henrik Lycksam for providing the opportunity to collect tomograms of the microstructure of wood using the XµCT scanner at the division of Fluid and Experimental Mechanics at Luleå University of Technology. The authors thank Emmy Lano for aiding in the segmentation and meshing of the tomograms of the microstructure of wood. The authors also thank all whom have provided high quality images for this publication.

Research ethics: Not applicable. Code availability: Not applicable

Author contributions: Conceptualization: Sara Florisson (SF), Kristofer Gamstedt (KG); methodology: SF, KG; software: SF; validation: SF; data curation: SF; formal analysis: SF; investigation: SF; resources: -; writing original draft: SF; writing, review & editing: SF, KG; visualization: SF; project administration: SF.

Competing interests: On behalf of all authors, the corresponding author states that there is no conflict of interest.

Research funding: Not applicable. Data availability: Not applicable.

References

- Akkus, Z., Galimzianova, A., Hoogi, A., Rubin, D., and Erickson, B.I. (2017). Deep learning for brain MRI segmentation: state of the art and future directions. J. Dig. Imaging 30: 449-459.
- Amrehn, M., Steidl, S., Kortekaas, R., Strumia, M., Weingarten, M., Kowarschik, M., and Maier, A. (2019). A semi-automated usability evaluation framework for interactive image segmentation systems. Int. J. Biomed. Imaging 2019. 1464592.
- Auenhammer, R.M., Mikkelsen, L.P., Asp, L.E., and Blinzler, B.J. (2021). Automated X-ray computed tomography segmentation method for finite element analysis of non-crimp fabric reinforced composites. Compos. Struct. 256: 113136.
- Auenhammer, R.M., Jeppesen, N., Mikkelsen, L.P., Dahl, V.A., Blinzler, B.J., and Asp, L.E. (2022). Robust numerical analysis of fibrous composites from X-ray computed tomography image data enabling low resolutions. Compos. Sci. Technol. 224. 109458.
- Autengruber, M., Lukacevic, M., and Füssl, I. (2020). Finite-element-based moisture transport model for wood including free water above the fibre saturation point. Int. J. Heat Mass. Transf. 161: 120228, https:// doi.org/10.1016/j.ijheatmasstransfer.2020.120228.
- Autengruber, M., Lukacevic, M., Gröstlinger, C., and Füssl, J. (2021). Finite-element-based prediction of moisture-induced crack patterns for cross sections of solid wood and glued laminated timber exposed to a realistic climate condition. Constr. Build. Mater. 271. 121775.
- Badel, E. and Perré, P. (2001). Using a digital X-ray imaging device to measure the swelling coefficients of a group of wood cells. Non Destr. Test. Eval. Int. 34: 345-353.
- Badel, E. and Perré, P. (2002). Predicting oak wood properties using X-ray inspection: representation, homogenisation and localisation. Part I: digital X-ray imaging and representation by finite elements. Ann. For. Sci. 59: 767-776.
- Baensch, F., Sause, M.G.R., Brunner, A.J., and Niemz, P. (2015). Damage evolution in wood - pattern recognition based on acoustic emission (AE) frequency spectra. Holzforschung 69: 357-365.
- Bay, B.K., Smith, T.S., Fyhrie, D.P., and Saad, M. (1999). Digital volume correlation: three dimensional strain mapping using X-ray tomography. Exp. Mech. 39: 217-226.
- Bengtsson, R., Afshar, R., and Gamstedt, E.K. (2022). An application orthotropic creep model for wood materials and composites. Wood Sci. Technol. 56: 1585-1604.
- Beucher, S. and Meyer, F. (1993). The morphological approach to segmentation: the watershed transformation. In: Dougherty, E.R. (Ed.). Mathematical morphology in image processing. Marcel Dekker Inc., New York, pp. 433-481.
- Boutelje, J.B. (1972). On the relationship between structure and the shrinkage and swelling of the wood in Swedish pine (Pinus silvestris) and spruce (Picea abies, Doctoral degree. Stockholm University, Stockholm, Sweden.
- Brandstätter, F., Autengruber, M., Lukacevic, M., and Füssl, J. (2023). Prediction of moisture-induced cracks in wooden cross sections using finite element simulations. Wood Sci. Technol. 57: 671-701.
- Brunke, O., Brockdorf, K., Drews, S., Müller, B., Donath, T., Herzen, J., and Beckmann, F. (2008). Comparison between X-ray tube based and synchrotron radiation based µCT. In: Optical engineering + applications. Engineering, S.T.I.S.f.O. SPIE: The International Society for Optical Engineering, San Diego, California, United States.

- Bryant, J.A., Drage, N.A., and Richmond, S. (2012). CT number definition. Radiat. Phys. Chem. 81: 358-361.
- Bucur, V. (2003). Ionizing radiation computed tomography. In: Nondestructive characterization and imaging of wood. Springer-Verlag, Berlin, Heidelberg, pp. 13-73.
- Buffiere, J.-Y., Maire, E., Adrien, J., Masse, J.-P., and Boller, E. (2010). Situ experiments with X ray tomography: an attractive tool for experimental mechanics, Exp. Mech. 50: 289-305.
- Buljac, A., Jailin, C., Mendoza, A., Neggers, J., Taillandier-Thomas, T., Bouterf, A., Smaniotto, B., Hild, F., and Roux, S. (2018). Digital volume correlation: review of progress and challenges. Exp. Mech. 58: 661-708.
- Carlsson, J. and Isaksson, P. (2020). Simulating fracture in a wood microstructure using a high-resolution dynamic phase field model. Eng. Fract. Mech. 232, 107030.
- Ching, D.J., Kamke, F.A., and Bay, B.K. (2018). Methodology for comparing wood adhesive bond load transfer using digitial volume correlation. Wood Sci. Technol. 52: 1569-1587.
- Cordes, N.L., Henderson, K., Stannard, T., Williams, J.J., Xiao, X., Robinson, M.W.C., Schaedler, T.A., Chawla, N., and Patterson, B.M. (2015). Synchroton-based X-ray computed tomography during compression loading of cellular materials. Microsc. Today 23: 12-19.
- Couceiro, J. (2019). X-ray computed tomography to study moisture distribution in wood, Doctoral degree. Division of Wood Science and Engineering, Luleå University of Technology, Skellefteå, Sweden.
- Couceiro, J., Hansson, L., Sehlstedt-Persson, M., Vikberg, T., and Sandberg, D. (2020). The conditioning regime in industrial drying of Scots pine sawn timber studied by X-ray computed tomography: a case-study. Eur. I. Wood Wood Prod. 78: 673-682.
- Couceiro, J., Hansson, L., Mannes, D., Niemz, P., and Sandberg, D. (2022). Estimation of the moisture content in wood by combination of neutron and X-ray imaging. In: 22nd international nondestructive testing and evaluation of wood symposium 2022, Quebec City, Canada.
- Cuete, D., Murphy, A. (2022). CT artifacts. [cited 2022 14 February]. Danvind, J. (2005). Analysis of drying wood based on nondestructive measurements and numerical tools. Doctoral degree. Department of Engineering Sciences and Mathematics, Division of Wood Science and Engineering, Luleå University of Technology, Skellefteå, Sweden.
- Derome, D., Griffa, M., Koebel, M., and Carmeliet, J. (2011). Hysteretic swelling of wood at cellular scale probed by phase-contrast X-ray tomography. J. Struct. Biol. 173: 180-190.
- de Ridder, M., van den Bulcke, J., Vansteenkiste, D., van Loo, D., Dierick, M., Masschaele, B., de Witte, Y., Mannes, D., Lehmann, E., Beeckman, H., et al. (2011). High-resolution proxies for wood density variations in Terminalia superba. Ann. Botany 107: 293-302.
- de Schryver, T., Dierick, M., Heyndrickx, M., van Stappen, J., Boone, M.A., van Hoorebeke, L., and Boone, M.N. (2018). Motion compensated micro-CT reconstruction for in-situ analysis of dynamic processes. Nat. Sci. Rep. 8: 7655.
- du Plessis, A., Tshibalanganda, M., and le Roux, S.G. (2020). Not all scans are equal: X-ray tomography image quality evaluation. Mater. Today Commun. 22. 100792.
- Eitelberger, J. and Hofstetter, K. (2011). A comprehensive model for transient moisture transport in wood below the fiber saturation point: physical background, implementation and experimental validation. Int. J. Therm. Sci. 50: 1861-1866.
- Eitelberger, J., Hofstetter, K., and Dvinskikh, S.V. (2011). A multi-scale approach for simulation of transient moisture transport processes in wood below the fiber saturation point. Compos. Sci. Technol. 71: 1727-1738.

- Ekevad, M. (2004). Method to compute fiber directions in wood from computed tomography images. J. Wood Sci. 50: 41-46.
- Endrizzi, M. (2018). X-ray phase-contrast imaging. Nucl. Instrum. Methods Phys. Res. Sect. A Accel. Spectrom. Detect. Assoc. Equip. 878: 88-98.
- Florisson, S. (2022). A methodology for miscroscopic computed tomography aided finite element modelling of wood. In: Conference proceedings of the 27th Swedish mechanics days (Svenska Mekanikdagar), 2022. Luleå University of Technology, Luleå, Sweden.
- Florisson, S., Vessby, J., Mmari, W., and Ormarsson, S. (2020). Threedimensional orthotropic nonlinear transient moisture simulation for wood: analysis on the effect of scanning curves and nonlinearity. Wood Sci. Technol. 54: 1197-1222.
- Florisson, S., Muszyński, L., and Vessby, J. (2021a). Analysis of hygro-mechanical behaviour of wood in bending. Wood Fiber Sci. 53:
- Florisson, S., Vessby, J., and Ormarsson, S. (2021b). A three-dimensional numerical analysis of moisture flow in wood and of the wood's hygro-mechanical and visco-elastic behaviour. Wood Sci. Technol. 55: 1269-1304.
- Florisson, S., Hansson, L., Couceiro, J., and Sandberg, D. (2022). Macroscopic X-ray computed tomography aided numerical modelling of moisture flow in sawn timber. Eur. J. Wood Wood Prod. 80: 1351-1365.
- Florisson, S., Hartwig, M., Wohlert, M., and Gamstedt, E.K. (2023). Microscopic computed tomography aided finite element modelling to estimate hygroexpansion coefficients of opposite and compression wood. Holzforschung 77: 700-712.
- Forsberg, F. (2008). X-ray microtomography and digital volume correlation for internal deformation and strain analysis, Doctoral thesis. Department of Applied Physics and Mechanical Engineering, Luleå University of Technology, Luleå, Sweden.
- Forsberg, F., Mooser, R., Arnold, M., Hack, E., and Wyss, P. (2008). 3D microscale deformations of wood in bending: synchrotron radiation µCT data analyzed with digital volume correlation. J. Struct. Biol. 164:
- Forsberg, F., Sjödahl, M., Mooser, R., Hack, E., and Wyss, P. (2010). Full threedimensional strain measurements on wood exposed to three-point bending: analysis by use of digital volume correlation applied to synchrotron radiation micro-computed tomography image data. Strain 46: 47-60.
- Fortino, S., Sippola, M., Andersson, T., Immonen, K., Miettinen, A., and Hradil, P. (2017). X-ray mico-tomography based FEM modelling of hygroexpansion in PLA composites reinforced with birch pulp fibers. Rakenteiden Mekaniikka 50: 131-136.
- Frandsen, H.L., Damkilde, L., and Svensson, S. (2007a). A revised multi-Fickian moisture transport model to describe non-Fickian effects in wood. Holzforschung 61: 563-572.
- Frandsen, H.L., Svensson, S., and Damkilde, L. (2007b). A hysteresis model suitable for numerical simulation of moisture content in wood. Holzforschung 61: 175-181.
- Fredriksson, M., Cool, J., and Avramidis, S. (2019). Automatic knot detection in coarse-resolution cone-beam computed tomography images of softwood logs. Forest Product J. 69: 185-187.
- Garcea, S.C., Wang, Y., and Withers, P.J. (2018). X-ray computed tomography of polymer composites. Compos. Sci. Technol. 156: 305-319.
- Greenway, K. and Gaillard, F. (2022). Hounsfield Unit.
- Hachem, C.E., Abahri, K., Vicente, J., Bennacer, R., and Belarbi, R. (2018). Hygromorphic characterization of softwood under high resolution X-ray tomography for hygrothermal simulation. Int. J. Heat Mass Tran. 54: 2761-2769.

- Hammerguist, C.C. and Nairn, J.A. (2018). Numerical simulation of pressuredriven adhesive penetration into realistic wood structures. Wood Sci. Technol. 52: 1271-1288.
- Hansson, L. and Cherepanova, E. (2012). Determination of wood moisture properties using a CT-scanner in a controlled low-temperature environment. Wood Mater. Sci. Eng. 7: 87-92.
- Hansson, L., Couceiro, J., and Fjellner, B.-A. (2016). Estimation of shrinkage coefficients in radial and tangential directions from CT images. Wood Mater. Sci. Eng. 12: 251-256.
- Hartig, J.H., Bieberle, A., Engmann, C., and Haller, P. (2021). Voxel-based finite element modelling of wood elements based on spatial density and geometry data using computed tomography. Holzforschung 75:
- Hattori, Y. and Kanagawa, Y. (1985). Non-destructive measurement of moisture distribution in wood with a medical X-ray CT scanner. Part 1: Accuracy and influencing factors. J. Japan Wood Res. Soc. (Mokuzai Gakkaishi) 31: 974.
- Hild, F., Bouterf, A., Chamoin, L., Leclerc, H., Mathieu, F., Neggers, J., Pled, F., Tomicevic, Z., and Roux, S. (2016). Toward 4D mechanical correlation. Adv. Model. Simul. Eng. Sci. 3: 17, https://doi.org/10.1186/s40323-016-
- Hofstetter, K., Hellmich, C., and Eberhardsteiner, J. (2005). Development and experimental validation of a continuum micromechanics model for the elasticity of wood. Eur. J. Mech. A/Solids 24: 1030-1053.
- Holmberg, S., Persson, K., and Petersson, H. (1999). Nonlinear mechanical behaviour and analysis of wood and fibre materials. Comput. Struct.
- Hsieh, J. (2015). Computed tomography: principles, design, artifacts and recent advances. Spie Press, Bellingham, Washington, USA.
- Hu, M., Olsson, A., Hall, S., and Seifert, T. (2022). Fibre directions at a branchstem junction in Norway spruce: a microscale investigation using X-ray computed tomography. Wood Sci. Technol. 56: 147–169.
- Huber, J.A.J., Broman, O., Ekevad, M., Oja, J., Hansson, L. (2022). A method for generating finite element models of wood boards from X-ray computed tomography scans. Compute. Struct. 260, 106702.
- Huč, S., Svensson, S., and Hozjan, T. (2018). Hygro-mechanical analysis of wood subjected to constant mechanical load and varying relative humidity. Holzforschung 72: 863-870.
- Huč, S., Svensson, S., and Hozjan, T. (2020). Numerical analysis of moistureinduced strains and stresses in glued-laminated timber. Holzforschung 74: 445-457.
- Joffre, T., Miettinen, A., Berthold, F., and Gamstedt, E.K. (2014). X-ray microcomputed tomography investigation of fibre length degradation during the processing steps of short-fibre composites. Compos. Sci. Technol. 105: 127-133.
- Joffre, T., Miettinen, A., Wernersson, E.L.G., Isaksson, P., and Gamstedt, E.K. (2017). Effects of defects on the tensile strength of short-fibre composite materials. Mech. Mater. 75: 125-134.
- Kamke, F.A., Nairn, J.A., Muszynski, L., Paris, J.L., Schwarzkopf, M., and Xiao, X. (2014). Methodology for micromechanical analysis of wood adhesive bonds using X-ray computed tomography and numerical modeling. Wood Fiber Sci. 46: 15-28.
- Kanagawa, Y. and Hattori, Y. (1985). Non-destructive measurement of moisture distribution in wood with a medical X-ray CT scanner. Part 2: Changes in moisture distribution with drying. J. Japan Wood Res. Soc. (Mokuzai Gakkaishi) 31: 983-989.
- Keunecke, D., Novosseletz, K., Lanvermann, C., Mannes, D., and Niemz, P. (2012). Combination of X-ray and digital image correlation for the

- analysis of moisture-induced strain in wood: opportunities and challenges. Eur. J. Wood Wood Prod. 70: 407-413.
- Keyak, J.H., Meagher, J.M., Skinner, H.B., and Mote, C.D., Jr. (1990). Automated three-dimensional finite element modelling of bone: a new method. J. Biomed. Eng. 12: 389-397.
- Keyak, J.H., Rossi, S.A., Jones, K.A., and Skinner, H.B. (1997). Prediction of femoral fracture load using automated finite element modeling. I. Biomech. 31: 125-133.
- Kibleur, P., Blykers, B., Boone, M.N., van Hoorebeke, L., van Acker, J., and van den Bulcke, J. (2022a). Detecting thin adhesive coatings in wood fiber materials with laboratory-based dual-energy computed tomography (DECT). Nat. Sci. Rep. 12: 15969.
- Kibleur, P., Manigrasso, Z., Goethals, W., Aelterman, J., Boone, M.N., van Acker, J., and van den Bulcke, J. (2022b). Microscopic deformations in MDF swelling: a unique 4D-CT characterization. Mater. Struct. 55: 206.
- Kollmann, F.F.P. and Côté, J.W.J. (1968). Principles of wood science and technology. Part I: Solid wood. Springer Verlag, Berlin.
- Kueh, A., Warnett, J.M., Gibbons, G.J., Brettschneider, J., Nichols, T.E., Williams, M.A., and Kendall, W.S. (2016). Modelling the penumbra in computed tomography. J. X-Ray Sci. Technol. 24: 583-597.
- Lazarescu, C., Watanabe, K., and Avramidis, S. (2010). Density and moisture profile evolution during timber drying by CT scanning measurements. Dry. Technol. 28: 460-467.
- Leclerc, H., Périé, J.-N., Fanget, A., Maire, E., Hild, F., and Roux, S. (2010). Microstructure-aided digital volume correlation, Vol. 6. E.W.o.C.
- Leclerc, H., Périé, J.-N., Hild, F., and Roux, S. (2012). Digital volume correlation: what are the limits to the spatial resolution? Mech. Ind. 13: 361-371.
- Lengsfeld, M., Schmitt, J., Alter, P., Kaminsky, J., and Leppek, R. (1998). Comparison of geometry-based and CT voxel-based finite element modelling and experimental validation. Med. Eng. Phys. 20: 515-522.
- Li, W., van den Bulcke, J., de Windt, I., van Loo, D., Dierick, M., Brabant, L., and van Acker, J. (2013). Combining electrical resistance and 3-D X-ray computed tomography for moisture distribution measurements in wood products exposed in dynamic moisture conditions. Build. Environ. 67: 250-259.
- Li, W., van den Bulcke, J., Mannes, D., Lehmann, E., de Windt, I., Dierick, M., and van Acker, J. (2014). Impact of internal structure on waterresistance of plywood studied using neutron radiography and X-ray tomography. Constr. Build. Mater. 73: 171-179.
- Li, W., van den Bulcke, J., de Schryver, T., and van Acker, J. (2016). Investigating water transport in MDF and OSB using a gantry-based X-ray CT scanning system. Wood Sci. Technol. 50: 1197–1211.
- Limodin, N., Réthoré, J., Adrien, J., Buffière, J.-Y., Hild, F., and Roux, S. (2011). Analysis and artifact correction for volume correlation measurements using tomographic images from a laboratory X-ray source. Exp. Mech. 51: 959-970.
- Lindgren, L.O. (1985). Preliminary observations on the relationship between density/moisture content in wood and X-ray attenuation in computerized axial tomography. In: Proceedings of the 5th NDT of wood symposium, 1985. Pullman, Washington, USA.
- Lindgren, L.O. (1988). Mätning av densitets- och fuktkvotsvariationer i trämaterial med datortomografi (Non-destructive measurements of density and moisture content variations in wood using computed tomography), Tech. Lic. thesis. Royal Institute of Technology, Stockholm, Sweden.
- Lindgren, L.O. (1991a). The accuracy of medical CAT-scan images for nondestructive density measurements in small volume elements within solid wood. Wood Sci. Technol. 25: 425-432.

- Lindgren, L.O. (1991b). Medical CAT-scanning: X-ray absorption coefficients, CT-numbers and their relation to wood density. Wood Sci. Technol. 25: 341-349.
- Lindgren, L.O. (1992). Medical CT-scanners for non-destructive wood density and moisture content measurements, Doctoral degree. Department of Wood Technology, Luleå University of Technology, Skellefteå, Sweden.
- Lindgren, O., Seifert, T., and Du Plessis, A. (2016). Moisture content measurements in wood using dual-energy CT scanning – a feasibility study. Wood Mater. Sci. Eng. 11: 312-317.
- Litjens, G., Kooi, T., Bejnordi, B.E., Setio, A.A.A., Ciompi, F., Ghafoorian, M., van der Laak, J.A.W.M., van Ginneken, B., and Sáchez, C.I. (2017). A survey on deep learning in medical image analysis. Med. Image
- Lobos, C., Payan, Y., and Hitschfeld, N. (2010). Techniques for the generation of 3D finite element meshes of human organs, ICI Global, Athens, Greece.
- Madi, K., Tozzi, G., Zhang, Q.H., Tong, J., Cossey, A., Au, A., Hollis, D., and Hild, F. (2013). Computation of full-field displacement in a scaffold implant using digital volume correlation and finite element analysis. Med. Eng. Phys. 35: 1298-1312.
- Maire, E. and Withers, P.J. (2014). Quantitative X-ray tomography. Int. Mater. Rev. 59: 1-43.
- Marks, L.W. and Gardner, T.N. (1993). The use of strain energy as a convergence criteria in the finite element modelling of bone and the effect of model geometry on stress convergence. J. Biomed. Eng. 15: 474-476.
- Martin, B., Colin, J., Perré, P., Casalinho, J., Mounkaila, M., Lu, P., and Rémond, R. (2022). CT investigation of 3D liquid pathways in the anatomical structure of Norway spruce wood during imbibition. Holzforschung 76: 592-603.
- McKinley, P.E., Ching, D.J., Kamke, F.A., Zauner, M., and Xiao, X. (2016). Micro X-ray computed tomography of adhesive bonds in wood. Wood Fiber
- Miettinen, A., Harjupatana, T., Kataja, M., Fortino, S., and Immonen, K. (2016). Time-resolved X-ray microtomographic measurement of water transport in wood-fibre reinforced composite material. In: 37th Risø international symposium on materials science, IOP Publishing, Risø, Denmark.
- Minaee, S., Boykov, Y., Porikli, F., Plaza, A., Kehtarnavaz, N., and Terzopoulos, D. (2022). Image segmentation using deep learning: a survey. IEEE Trans. Pattern Anal. Mach. Intell. 44: 3523-42.
- Modzel, G.G.R. (2009). Computed tomography analysis of wood-adhesive bonds, Doctoral degree. Department of Wood Science and Engineering, Oregon State University, Corvallis, United States.
- Murphy, A. and Haouimi, A. (2022). Image reconstruction (CT).
- Otsu, N. (1979). A threshold selection method from gray-level histograms. IEEE Trans. Syst. Man Cybern. 9: 62-66.
- Oudjene, M. and Khelifa, M. (2009). Elasto-plastic constitutive law for wood behaviour under compressive loadings. Constr. Build. Mater. 23: 3359-3366.
- Pagès, A., Sermesant, M., Frey, P. (2005) Generation of computational meshes from MRI and CT-scan data. ESAIM Proc. 14: 213-223.
- Pak, D.H., Liu, M., Ahn, S.S., Caballero, A., Onofrey, J.A., Liang, L., Sun, W., Duncan, J.S. (2021). Weakly supervised deep learning for aortic valve finite element mesh generation from 3D CT images. Inf. Proces. Med. Imaging. https://doi.org/10.1007/978-3-030-78191-0_49.
- Pan, J., Huang, J., Cheng, G., and Zeng, Y. (2023). Reinforcement learning for automatic quadrilateral mesh generation: a soft actor-critic approach. Neural Network. 157: 288-304.

- Paris, J.L., Kamke, F.A., Mbachu, R., and Kraushaar Gibson, S. (2014). Phenol formaldehyde adhesives formulated for advanced X-ray imaging in wood-composite bondlines. J. Mater. Sci. 49: 580-591.
- Paris, J.L., Kamke, F.A., and Xiao, X. (2015). X-ray computed tomography of wood-adhesive bondlines: attenuation and phase-contrast effects. Wood Sci. Technol. 49: 1185-1208.
- Patera, A., Carl, S., Stampanoni, M., Derome, D., and Carmeliet, J. (2018a). A non-rigid registration method for the analysis of local deformations in the wood cell wall. Adv. Struct. Chem. Imaging 4: 1, https://doi.org/ 10.1186/s40679-018-0050-0.
- Patera, A., van den Bulcke, J., Boone, M.N., Derome, D., and Carmeliet, J. (2018b). Swelling interactions of earlywood and latewood across a growth ring: global and local deformations. Wood Sci. Technol. 52: 91_114
- Pech, S., Lukacevic, M., and Füssl, J. (2021). A robust multisurface returnmapping algorithm and its implementation in Abagus. Finite Elem. Anal. Des. 190. 103531.
- Perré, P., Nguyen, D.M., and Almeida, G. (2022). A macroscopic Washburn approach of liquid imbibition in wood derived from X-ray tomography observations. Sci. Rep. 12, https://doi.org/10.1038/s41598-022-05508-0.
- Persson, K. (2000). Micromechanical modelling of wood and fibre properties, Doctoral degree. Department of Mechanics and Materials, Lund University, Lund, Sweden.
- Pyrkosz, M., van Karsen, C., Bissinger, G. (2010). Converting CT scans of a Stradivari violin to a FEM. In: IMAC conference on structural dynamics. https://10.1007/978-1-4419-9834-7.
- Rosenkilde, A. (2002). Moisture content profiles and surface phenomena during drying of wood, Doctoral degree. Royal Institute of Technology, Stockholm, Sweden.
- Roux, S., Taillandier-Thomas, T., Bouterf, A., Leclerc, H., Morgeneyer, T.F., and Hild, F. (2012). Digital volume correlation from tomographic images: results and challenges. In: IUTAM symposium on advances of optical methods in experimental mechanics.
- Russ, J.C. and Neal, F.B. (2016). The image processing handbook. CRC Press. Salin, J.-G. (1992). Numerical prediction of checking during timber drying and a new mechano-sorptive creep model. Eur. I. Wood Prod. 50: 195-200.
- Salvo, L., Cloetens, P., Maire, E., Zabler, S., Blandin, J.J., Buffiere, J.Y., Ludwiq, W., Boller, E., Bellet, D., and Josserond, C. (2003). X-ray microtomography an attractive characterisation technique in material science. Nucl. Instrum. Methods Phys. Res. B: Beam Interact. Mater. Atoms 200: 273-286.
- Sehlstedt-Persson, M. (2001). The effect of extractive content on moisture diffusion properties for Scots pine and Norway spruce. In: OST action E15 advances in the drying of wood. Proceedings 3rd workshop on softwood drying to specific end-uses. Finland, Helsinki.
- Seibert, J.A., Boone, J.M., Lindfors, K.K. (1998). Flat-field correction technique for digital detectors. In: Medical imaging, 1998. San Diego,
- Seo, H., Khuzani, M.B., Vasudevan, V., Huang, C., Ren, H., Xiao, R., Jia, X., and Xing, L. (2020). Machine learning techniques for biomedical image segmentation: an overview of technical aspects and introduction to state-of-art applications. Med. Phys. 47: 148-167.
- Sisodia, S.M., Bull, D.J., George, A.R., Gamstedt, E.K., Mavrogordato, M.N., Fullwood, D.T., and Spearing, S.M. (2019). The effects of voids in quasistatic indentation of resin-infused reinforced polymers. J. Compos. Mater. 53: 4399-4410.
- Song, R., Liu, J., and Cui, M. (2017). A new method to reconstruct structured mesh model from micro-computed tomography images of porous media and its application. Int. J. Heat Mass Transfer 109: 705-715.
- Srinivasa, P. (2017). Mechanics of nanocellulose foams: experimental and numerical studies, Doctoral degree. Department of Solid Mechanics, KTH School of Engineering Sciences Stockholm, Sweden.

- Stock, S.R. (2013). Recent advances in X-ray microtomography applied to materials. Int. Mater. Rev. 53: 129-181.
- Stubbs, C.J., Larson, R., and Cook, D.D. (2020). Mapping spatially distributed material properties in finite element models of plan tissue using computed tomography. Biosyst. Eng. 200: 391-399.
- Taddei, F., Pancanti, A., and Viceconti, M. (2004). An improved method for the automatic mapping of computed tomography numbers onto finite element models. Med. Eng. Phys. 26: 61-69.
- Thermo Fisher Scientific. (2022). User's guide Avizo 3D 2021-2.
- Tran, H., Doumalin, P., Delisee, C., Dupre, J.C., Malvestio, J., and Germaneau, A. (2013). 3D mechanical analysis of low-density wood-based fibreboards by X-ray microcomputed tomography and digital volume correlation. J. Mater. Sci. 48: 3198-3212.
- van Dijk, N.P., Wu, D., Persson, C., and Isaksson, P. (2019). A global digital volume correlation algorithm based on higher-order finite elements: implementation and evaluation. Int. J. Solids Struct. 168:
- Verho, T., Fortino, S., Hradil, P., Turpeinen, T., Immonen, K., Harlin, A., and Sandquist, D. (2022). Biocomposite modeling by tomographic feature extraction and synthetic microstructure reconstruction. Compos. Sci. Technol. 230. 109713.
- Viceconti, M., Bellingeri, L., Cristofolini, L., and Toni, A. (1998). A comparative study on different methods of automatic mesh generation of human femurs. Med. Eng. Phys. 20: 1-10.
- Wang, L., Chitiboi, T., Meine, H., Günther, M., and Hahn, H.K. (2016). Principles and methods for automatic and semi-automatic tissue segmentation in MRI data. Magn. Reson. Mater. Phys. Biol. Med. 29: 95-110.
- Wang, B., Pan, B., Tao, R., and Lubineau, G. (2017). Systematic errors in digital volume correlation due to the self-heating effect of a laboratory X-ray CT scanner. Meas. Sci. Technol. 28. 055402.
- Watanabe, K., Lazarescu, C., Shida, S., and Avramidis, S. (2012). A novel method of measuring moisture content distribution in timber drying using CT scanning and image processing techniques. Dry. Technol.
- Wiberg, P. (1998). CT-scanning of moisture distributions and shell formation during wood drying, Doctoral degree, Division of Wood Physics, Luleå University of Technology, Skellefteå, Sweden.
- Withers, P.J., Bouman, C., Carmignato, S., Cnudde, V., Grimaldi, D., Hagen, C.K., Maire, E., Manley, M., Du Plessis, A., and Stock, S.R. (2021). X-ray computed tomography. Nat. Rev. 1: 18, https://doi.org/ 10.1038/s43586-021-00015-4.
- Yu, T., Khaloian, A., and van de Kuilen, J.-W. (2022). An improved model for the time-dependent material response of wodo under mechanical loading and varying humidity conditions. Eng. Struct. 259. 114116.
- Zauner, M. (2014). In-situ synchrotron based tomographic microscopy of uniaxially loaded wood: in-situ testing device, procedures, and experimental investigations, Doctoral degree. Institute for Building Materials, Swiss Federal Institute of Technology Zurich, Switzerland.
- Zauner, M., Stampanoni, M., and Niemz, P. (2016). Failure and failure mechanisms of wood during longitudinal compression monitored by synchrotron micro-computed tomography. Holzforschung 70: 179-185.
- Zhong, W., Zhang, Z., Chen, X., Wei, Q., Chen, G., and Huang, X. (2021). Multiscale finite element simulation on large deformation behavior of wood under axial and transverse compression conditions. Acta Mechanica Sinica 37: 1136-1151.
- Zink, A.G., Davidson, R.W., and Hanna, R.B. (1995). Strain measurement in wood using a digital image correlation technique. Wood Fiber Sci. 27:
- Zwanenburg, E.A., Williams, M.A., and Warnett, J.M. (2022). Review of highspeed imaging with lab-based X-ray computed tomography. Meas. Sci. Technol. 33. 012003.